Michigan Technological University
Digital Commons @ Michigan Tech

Dissertations, Master's Theses and Master's Reports

2022

Optimal Control of Nonlinear Wave Energy Converters In Heave for Maximum Power Extraction

Kevin Nelson
Michigan Technological University, knelson@mtu.edu

Copyright 2022 Kevin Nelson

Recommended Citation

Nelson, Kevin, "Optimal Control of Nonlinear Wave Energy Converters In Heave for Maximum Power Extraction", Open Access Master's Thesis, Michigan Technological University, 2022.
https://doi.org/10.37099/mtu.dc.etdr/1469

Follow this and additional works at: https://digitalcommons.mtu.edu/etdr
Part of the Energy Systems Commons, and the Ocean Engineering Commons

OPTIMAL CONTROL OF NONLINEAR WAVE ENERGY CONVERTERS IN HEAVE FOR MAXIMUM POWER EXTRACTION

By

Kevin Nelson

A THESIS

Submitted in partial fulfillment of the requirements for the degree of

MASTER OF SCIENCE

In Mechanical Engineering

MICHIGAN TECHNOLOGICAL UNIVERSITY

2022

© 2022 Kevin Nelson

This thesis has been approved in partial fulfillment of the requirements for the Degree of MASTER OF SCIENCE in Mechanical Engineering.

Department of Mechanical Engineering - Engineering Mechanics

Thesis Advisor: *Dr. Gordon Parker*

Committee Member: *Dr. Wayne Weaver*

Committee Member: *Dr. Guy Medows*

Department Chair: *Dr. Jason Blough*

Dedication

To my Fiancee

without her immense support in the home stretch, I would not have completed this work,

and to my Family

whose love and encouragement shaped me into the person I am today.

Contents

List of Figures . . . . **xi**

List of Tables . . . . **xv**

Acknowledgments . . . . **xvii**

Abstract . . . . **xix**

1 Introduction **1**

- 1.1 Organization of this Thesis 5
- 1.2 Motivation 7
- 1.3 Background 9
  - 1.3.1 Demand for Renewable Resources 9
  - 1.3.2 A Selection of Wave Energy Converter Types 11
  - 1.3.3 Parts of a WEC 12
  - 1.3.4 Hydrostatic and Hydrodynamic Interactions 13
  - 1.3.5 Control 15
- 1.4 Overview of Optimal Control Theory 17
  - 1.4.1 Optimal Control Problem Formulation 17

1.4.2 Pontryagin's Minimum Principle 20

1.4.3 Singular Arcs 22

1.4.4 Necessary Conditions 23

1.4.5 Generalized Legendre-Clebsch Conditions for Singular Arcs . 25

2 Optimal Control of a General Class of Non-linear WECs 27

2.1 Dynamic System Model 28

2.2 General Optimal Control Solution 32

2.3 Legendre-Clebsch Necessary Conditions 40

2.4 Relationship Between Optimal Solution and Conjugate Control . . . 42

2.4.1 Derivation of Complex Conjugate Control 43

2.4.2 Relationship with Optimal Control 47

2.5 Application to Linear Buoy Model 49

2.5.1 Application of General Control Law to Linear Buoy 50

2.5.2 Optimal Initial Conditions 54

2.5.3 Numerical Simulation on Singular Arc 56

2.5.4 Numerical Simulation off of Singular Arc 62

2.6 Application to Hour Glass Buoy 72

2.6.1 Application of General Control Law to Hourglass Buoy . . . 73

2.6.2 Searching for Singular Arcs 78

2.6.3 Numerical Simulation of Hourglass Buoy 79

3 Conclusions 89

3.1 Summary of Findings 89

3.2 Future Work 91

References 93

A Differentiable Approximations to Piecewise Linear Functions . . 97

A.1 Approximation of the Saturate Function 100

A.2 Approximation of the Abs Function 101

B Mathematica Code 103

List of Figures

2.1 Free body diagram of simple dynamic model 29

2.2 Free body diagram of simple dynamic model 31

2.3 Position and velocity of the buoy vs time 57

2.4 Velocity and control force of the buoy vs time. Note that velocity is given in decimeters/second, and control force is given in kilonewtons to make graph scales comparable. The wave field frequency is set at the resonant frequency of the buoy 58

2.5 Instantaneous and average extracted power from the buoy vs time . 59

2.6 Hamiltonian vs time 60

2.7 Switching function ζ vs time 61

2.8 Co-state numerically integrated (evolved) from the differential equation and calculated from the singular arc constraint 62

2.9 Position and velocity vs time with initial conditions $(x0, v0) \approx (0.273, 0)$ 63

2.10 Velocity and control force vs time with initial conditions $(x0, v0) \approx (0.273, 0)$. Note that velocity is given in decimeters/second, and control force is given in kilonewtons to make graph scales comparable. . . 64

2.11 Instantaneous and average extracted power from the buoy vs time with initial conditions $(x0, v0) \approx (0.273, 0)$ 65

2.12 Switching function ζ vs time with initial conditions $(x0, v0) \approx (0.273, 0)$ 66

2.13 Co-state numerically integrated (evolved) from the differential equation and calculated from the singular constraint with initial conditions $(x0, v0) \approx (0.273, 0)$ 67

2.14 Position and velocity vs time with initial conditions $(x0, v0) = (0, 0)$ 69

2.15 Velocity and control force vs time with initial conditions $(x0, v0) = (0, 0)$. Note that velocity is given in decimeters/second, and control force is given in kilonewtons to make graph scales comparable. . . 70

2.16 Instantaneous and average extracted power from the buoy vs time with initial conditions $(x0, v0) = (0, 0)$ 71

2.17 Co-state numerically integrated (evolved) from the differential equation and calculated from the singular constraint with initial conditions $(x0, v0) = (0, 0)$ 72

2.18 Schematic representation of an hourglass buoy 73

2.19 Phase space of hourglass buoy at t=7 s with two found singular arcs 80

2.20 Phase space of hourglass buoy at t=10.5 s with two found singular arcs 81

2.21 Velocity and control force for large (orange) singular arc orbit . . . 82

2.22 Instantaneous and Average power for large (orange) singular arc orbit 83

2.23 Co-state evolved vs constraint check for large (orange) singular arc orbit 84

2.24 Velocity and control force for smaller (blue) singular arc orbit . . . 85

2.25 Velocity and control force for smaller (blue) singular arc orbit . . . 86

2.26 Velocity and control force for smaller (blue) singular arc orbit . . . 87

A.1 Saturate(x) and Abs(x) and their derivatives 98

A.2 Step(x) function overlaid against Sigmoid(x) curve with k=50 . . . 99

List of Tables

2.1 Numerical values of quantities used in linear simulations 56

2.2 Numerical values of quantities used in nonlinear simulations 80

Acknowledgments

I would like to acknowledge my advisor Dr. Gordon Parker who has been patient, kind, and and an endless source of knowledge as I have completed the work on this topic.

I would also like to acknowledge Dr. Wayne Weaver who is an expert in optimal control theory and taught the special topics class from which the topic of this thesis was born.

Finally, I would like to acknowledge Houssein Yassin whose parallel work aided in the development of several of the ideas found in this thesis.

Abstract

The marine renewable energy community is interested in maximizing the power generated by nonlinear wave energy converters. Optimal control methods provide a tool to achieve this aim and can also help to inform the buoy design. An energy-optimal control law for a class of non-linear buoy models is derived and is shown to be singular. The solution approach is illustrated using an hourglass-shaped buoy having a cubic, hydrostatic nonlinearity. The optimal control law is only valid on singular arcs, and a method to search for these arcs is presented. Two singular arcs are found for the hourglass buoy model and analyzed. Neither is likely optimal thus, finding the energy-optimal singular arc is left for future work.

Chapter 1

Introduction

In this thesis, optimal control methods are explored for extracting the maximum amount of power from both linear and nonlinear, point absorber wave energy converters (WECs). The analysis focuses on axisymmetric wave energy converter buoys in heave, although the methods presented may have applications elsewhere.

For the optimal control problem to be tractable, only a specific class of non-linear forces is considered. This class of nonlinear forces is important to the wave energy community because many hydrostatic and hydrodynamic interactions of interest between the buoy and the water surface fit into this class and can be used in the analysis presented.

It is shown that the optimal control that maximizes extracted energy falls into a particular class called singular arc control solutions. This class of optimal control problems requires specific consideration which is detailed in this thesis. However, the fact that the problem is singular ends up being fortuitous as this allows a general control law can be derived. This control law is considered general because it can be applied to any dynamic system model which fits into the class of non-linear forces which is considered. The analysis deriving this general control law is the main result of this thesis.

For the general control law to be valid, the system must be on a singular arc. Of the infinite set of possible trajectories which exist that the system can be on, only a small subset meets the criteria of being singular. There exists a criterion called the stationary condition, which if met classifies a trajectory as singular. This means that certain initial conditions must be chosen so that the system starts on one of these singular arcs. If the system starts on a singular arc, the general control law will force the system to remain on that arc.

Analysis is done to show that one of the singular arcs maximizes the power extracted from the device. A second-order test called the general Legendre-Clebsch condition is performed to show that being on a singular arc is a necessary condition for maximizing the power extraction.

When the buoy is not on a singular arc, power extraction is not maximized. In this case, bang-bang control can be used to drive the system to a singular arc. Once the system has reached the singular arc, the optimal control law may be used to keep the system on that arc. Pontryagin's Minimum Principle is discussed, and it follows from this principle that bang-bang control is optimal when the system is not on the singular arc.

To perform bang-bang control, a switching function must be defined. This switching function should drive the system to the singular arc. For instance, if the switching function is positive, the maximum control force is applied, if the switching function is negative, the minimum control force is applied, and if the switching function is identically 0 then the system is on the singular arc and the general control law can be used. It is assumed that the available control force is symmetric, i.e the maximum control force equals the negative of the minimum control force. This assumption is not required by the analysis but is typical in real-world applications.

One of the first forms of control ever explored in the wave energy field is called complex conjugate control. This type of control essentially forces a linear buoy to operate at resonance, which maximizes the velocity of the buoy. Then, the well-known result of impedance matching is used to maximize the power extracted from the buoy. This form of control was valid for linear buoys in regular waves i.e. waves that are modeled by a sinusoid at a single frequency. It is shown analytically that complex conjugate control is a special case of the optimal control law developed in this thesis.

The optimal control law is applied to a linear model of a buoy. The linear model is shown to be a special case of the class of non-linear models which are studied. This is a "toy" model as it is not predictive of many buoys which are used in the real world. However, the interaction between the general control law and the linear buoy is rich enough to gain an intuitive understanding of how more realistic problems will act. A switching function is found for the linear buoy model, and numerical analysis using this switching function is explored. The behavior of the linear buoy with bang-bang and singular control is explored extensively.

The general control law is then applied to an hour-glass shaped buoy. This demonstrates how non-linear buoy shapes may be used in the optimal control analysis. Only hydrostatic forces are considered in this analysis, although in principle nothing is preventing hydrodynamic forces from being included. Difficulties in finding a switching function for the hourglass buoy are discussed.

An infinite number of singular arcs are shown to exist, and only one of these arcs will maximize the power extracted from the device. It is shown that the singular arc which maximizes the power extraction can be found through numerical simulation. Future work may be done to find a systematic approach to finding the arc which maximizes power extraction.

1.1 Organization of this Thesis

Section 1.2, entitled ”Motivation”, provides a more detailed explanation of why the optimal control law derived in this thesis is important to the wave energy community.

Section 1.3, entitled ”Background”, provides an overview of why wave energy is important in combating climate change. It then provides a general overview of the different types of wave energy converters. The basic components of a wave energy converter are covered. A case for applying closed-loop control to wave energy converters is made. Finally, the optimal control of wave energy converters is discussed.

Section 1.4 discusses the theoretical framework for developing an optimal control problem. An important set of necessary conditions known as the Euler-Lagrange equations are derived. Pontryagin’s Minimum Principal is discussed, as is the definition of a singular arc problem. The necessary conditions for optimality including the stationary condition and the Legendre-Clebsch conditions are discussed. Finally, a generalized Legendre-Clebsch test is discussed which works for singular arc problems.

Chapter 2 discusses the optimal control of both linear and non-linear wave energy converters.

Section 2.1 goes over the class of dynamic system models which will be considered in this thesis.

Section 2.2 shows the general solution for developing an optimal control law that keeps a general class of non-linear dynamic buoy models on the optimal singular arc. Showing that an optimal singular arc exists for this class of non-linear buoys is the main contribution of this thesis.

Section 2.3 shows that the optimal solution derived in 2.2 passes the general 2nd order Legendre-Clebsch test for singular arcs. This is a necessary condition for the solution to be a local minimum over the singular arc. The fact that the general control law passes the Legendre-Clebsch test over the class of non-linear models is new work in this thesis.

In section 2.4, an equivalency is shown between the optimal solution for a linear buoy and complex conjugate control. Zou et al. showed that the numerical simulation of the optimal control law and the buoy were equivalent [1]. This thesis extends that by showing an analytical derivation of the equivalency.

In section 2.5, the general control law is applied to a linear buoy, and the resulting control law is shown to be identical to what Zou et al. reached in their paper [1]. Numerical simulation is shown of how the system acts when the initial conditions are started both on and off of the optimal singular arc. New work is completed to show through analysis and simulation that there are an infinite number of singular arcs and that only one is optimal. Because it is clear when the power extraction of the linear model is maximized, a simple numerical scheme is used to find the optimal singular arc.

Section 2.6 shows new work to apply the general control law to an hourglass-shaped buoy. This section discusses how to apply the general control law to a non-linear example. Only hydrostatic forces are considered for simplicity. There is no reason in principle why the method presented could not be extended to hydrodynamic forces. A numerical method for searching for singular arcs is presented, and two candidates are found. Each arc is analyzed for power generation. It is unlikely that either arc is the optimal candidate.

In chapter 3 a summary of findings and future work can be found.

1.2 Motivation

The main contribution of this thesis is to show a method of formulating an optimal control law for a wide variety of non-linear wave energy converters. When applied to a wave energy converter model, this control law will force the system to evolve along an optimal trajectory. The trajectory is optimal in that the total power extracted from the system is maximized over this trajectory.

Consider an axisymmetric buoy oscillating in heave. Let m be the mass of a buoy, ζ be the position of the buoy in heave, b be the linear viscous damping, k be the spring force, $f_e(t)$ be the excitation force, and u be the control force. For the linear model described below in equation 1.1, there exists an optimal control function u which keeps the system on the optimal trajectory [1]. This control function will be derived later in section 2.5.

$$m\ddot{\zeta} + b\dot{\zeta} + k\zeta = f_e(t) - u \tag{1.1}$$

This thesis considers a broader class of non-linear models, where the spring force and excitation terms can be described by any potentially non-linear function $f_nl(\zeta, t)$.

$$m\ddot{\zeta} + c\dot{\zeta} = f_{nl}(\zeta, t) - u \tag{1.2}$$

Note that the linear model of equation 1.1 is a special case of the non-linear model in equation 1.2 where $f_{nl}(zeta, t) = f_e(t) - k\,\zeta$.

The non-linear force term $f_{nl}(\zeta, t)$ admits a variety of interesting phenomena including modeling the nonlinear forces arising from non-cylindrical buoys experiencing large displacements.

This work shows that there is a general optimal control law that can be applied to nonlinear point absorbers experiencing large motions. The law is only valid when the system is on a singular arc. A method for searching for singular arcs is presented. If the optimal singular arc candidate can be found, then it can then be used to build tracking control laws. In addition, it can be used for designing energy-optimal buoy shapes.

Future work needs to be done to be able to find these trajectories for non-linear systems systematically.

1.3 Background

Wave energy is likely to play an important role in the future of renewable energy. The demand for renewable resources is high and will likely need to be filled by a variety of sources. Wave energy converters offer an additional resource that may be able to ease the growth requirements of traditional wind, solar, and hydro renewable sources.

1.3.1 Demand for Renewable Resources

Total US energy production in 2013 was about 3.7 terawatt years (TWy) [2]. Approx 9% of that amount was supplied by renewable energy.

At the current rate of growth, the US will produce about 8.65 TWy in 2050 [3]. Energy models show that between 28% and 74% of this total energy will need to come from renewable sources to meet climate mitigation and pollution objectives [4]. An average figure of 50% renewable energy production requires the addition of 100 gigawatt years (GWy) of renewable energy every year starting in 2014. Scaling the current US renewable energy portfolio, made of hydroelectric, geothermal, solar, wind, and biomass sources, to this amount, would require significant additional resource utilization. These rates would require the **annual** addition of 90 billion tons of water falling from 1000 m, about 1580 km^2 of new PV panel area, and about 180 km^2 of new turbine swept area [3]. Offshore energy provides a significant additional resource that could ease the growth curves of other renewable resources.

The following figures help to get a sense of how much energy is available from wave energy sources. Wave energy is typically measured in kilowatts per meter of wave front. Approximately 37 kW/m is available off the US Northern Pacific coast, and 33 kW/m is available off the US Northern Atlantic coast [5]. It is estimated that approximately 590 TWh/year can be extracted from the West Coast, and approximately 230 TWh/year of energy can be extracted from the East Coast [3]. In general, more power is available at high northern or southern latitudes, especially in the winter months [3]. From the figures above, it can be seen that wave energy can play an important role in the future demand for renewable energy sources.

1.3.2 A Selection of Wave Energy Converter Types

Many different types of wave energy converters have been studied to harness wave energy in different environments. A short synopsis of several interesting buoys is provided below.

One of the earliest devices was the tail-tube or pneumatic buoy, also called an oscillating water column buoy [3]. This device consists of a cylindrical buoy with a deeply immersed central tube. The tube creates a central shaft of water which was isolated from the wave motion. This shaft of water can be used to produce relative motion against the buoy as it heaved up and down in the wave field. Navigation buoys using this principle to generate power were used in Japan as early as the 1940s [6].

The Edinburgh Duck was a novel buoy concept developed by Professor Steven Salter at the University of Edinburgh in the 1970s [3]. The duck was specifically designed to extract energy in a beam-sea configuration. The shape was optimized to ”terminate” the wave, and energy conversion efficiency could approach 100% in correct wave conditions [3]. A weakness of the duck design is that the efficiency of the device was significantly degraded if the wavefront was not perpendicular to the device [3].

Axisymmetric point absorber buoys are the main object of analysis in this thesis. They prove popular as many methods of analysis are available, and often these types of buoys can be the easiest to construct and install. An interesting feature of these buoys is that they can absorb more energy than is directly incident on the diameter of the buoy [3]. This feature is wavelength dependent, and the maximum characteristic length that they can absorb over is found as $\lambda\, d/2\pi$ where λ is the wavelength of the wave field, and d is the diameter of the buoy [7].

1.3.3 Parts of a WEC

The main goal of a wave energy converter is to generate relative motion from the oscillatory force generated from waves. This motion then can be used to generate power. This thesis will mainly consider WECs that float out at sea. Other types of devices do exist, for instance, WECs that are built into break walls near the shore.

Wave energy converters usually consist of a floating body, some kind of mooring system, and a power-take-off unit, which is responsible for generating power. Many power-take-off unit designs exist, these may be hydraulic pumps, linear/rotary generators, or turbine systems [3]. The power lines are usually run through the mooring system to the sea floor where they connect with an underwater power grid.

1.3.4 Hydrostatic and Hydrodynamic Interactions

For a heaving point absorber, the most relevant non-linear component of the hydrodynamic force is the Froude-Krylov force [8]. This force is the integration of the incident pressure from the water over the wetted surface of the buoy [8].

The Froude-Krylov can be broken down into a static and a dynamic component, yielding the hydrostatic and the hydrodynamic forces of the buoy respectively. The Froude-Krylov forces can be computed as follows:

$$f_{fk} = \iint_{S(t)} P\,\mathbf{n}\,dS \tag{1.3}$$

where P is the pressure over the wetted surface, $\mathbf{n}$ is the normal over the wetted surface, and $S(t)$ is the area of the wetted surface. Therefore dS is an infinitesimal patch of the wetted surface.

The pressure can be estimated using Airy's wave theory for deep water waves [8]:

$$P = \rho\, g\, a\, e^{\chi\, z}\, \cos(\omega\, t - \chi\, x) - \rho\, g\, z \tag{1.4}$$

where a is the amplitude of the wave, χ is the wavenumber, z is the vertical direction, ω is the frequency, and x is the direction of propagation.

Airy's wave theory can be split up into static and dynamic components as shown below:

$$P_{dy} = \rho\, g\, a\, e^{\chi\, z}\, \cos(\omega\, t - \chi\, x) \tag{1.5}$$

$$P_{st} = -\rho\, g\, z \tag{1.6}$$

This leads naturally to splitting the integral in equation 1.3 into two parts as follows:

$$f_{fk,dy} = \iint_{S(t)} P_{dy}\, \mathbf{n}\, dS = \rho\, g\, a \iint_{S(t)} e^{\chi\, z}\, \cos(\omega\, t - \chi\, x)\, \mathbf{n}\, dS \tag{1.7}$$

$$f_{fk,st} = \iint_{S(t)} P_{st}\, \mathbf{n}\, dS = -\rho\, g \iint_{S(t)} z\, \mathbf{n}\, dS \tag{1.8}$$

where $f_{fk,dy}$ are the Froude-Krylov hydrodynamic forces, and $f_{fk,st}$ are the Froude-Krylov hydrostatic forces.

These integrals then need to be evaluated for the particular buoy shape under consideration.

1.3.5 Control

Applying closed-loop control to wave energy converters can increase their power output by a factor of 3-5 fold [3]. Oftentimes, the necessary control force can be introduced into a buoy through the existing power-take-off unit, yielding the advantages of control with minimal cost.

An early type of control applied to buoys was called complex conjugate control (also known as impedance matching) [9]. The idea behind complex conjugate control was to force the buoy to operate at resonance by using the control force to cancel the mass and spring terms in the dynamic system equation [10]. Then the maximum power would be transferred from the buoy if the damping in the power-take-off unit matched the damping in the buoy system [3].

Optimal Control methods have been applied to wave energy converters. These methods are useful because they can provide upper theoretical bounds on the amount of energy that can be extracted from a device. Zou et al. adapted a result from the optimal control of vibration dampers to show how to maximize the power drawn from a linear WEC buoy [1] [11]. Zou et al. showed that the optimal trajectory is singular for their model because the Hamiltonian is linear in the control function [1]. They also show that utilizing the optimal control law for the singular trajectory is more optimal than traditional bang-bang controllers [1]. Finally, they compare simulations of their method against complex conjugate control [1].

This thesis shows that similar optimal control methods to those in Zou et al. can be used on a wider class of non-linear buoy models [1]. This wider class of models can include important non-linear dynamics such as the static and dynamic Freude-Krylov forces for many axisymmetric buoy shapes, although only the static forces are analyzed in this thesis.

This thesis shows that extracted power is maximized when the system is on the singular trajectory, as well as deriving a general control law that will keep the system on the optimal singular trajectory. It also discusses the difficulty in finding the singular arc for non-linear systems (specifically an hour-glass buoy is analyzed), as well as the difficulty in finding a switching function that can be utilized with bang-bang control to drive the system to the singular arc.

1.4 Overview of Optimal Control Theory

The goal of optimal control theory is to determine an admissible control function that yields an optimal trajectory. The trajectory is considered optimal if it minimizes a given cost function while obeying a given set of constraints.

In the particular formulation followed in this thesis, the cost function will relate to the energy extracted from the buoy, and the constraints will force the optimal trajectory to obey the differential system of equations that describes the buoy motion.

1.4.1 Optimal Control Problem Formulation

Note that for clarity of reading, boundary terms have been omitted as they do not affect the derivation of the particular optimal control problem studied.

Let $\phi(\boldsymbol{x}(t), \boldsymbol{u}(t), t)$ be an arbitrary Lagrangian to minimize and $\dot{\boldsymbol{x}}(t) = \boldsymbol{f}(\boldsymbol{x}(t), \boldsymbol{u}(t), t)$ be a set of dynamic equations which describe a system of interest.

Then J, which is a cost function to be minimized, can be defined as:

$$J = \int_{t_0}^{t_f} \phi(\boldsymbol{x}(t), \boldsymbol{u}(t), t) + \boldsymbol{\lambda}(t)^T \left[\boldsymbol{f}(\boldsymbol{x}(t), \boldsymbol{u}(t), t) - \dot{\boldsymbol{x}}(t)\right],\ dt \tag{1.9}$$

The integrand of the above cost function is composed of the sum of the Lagrangian and a set of equality constraints that are adjoined to the cost function through Lagrange multipliers. The Lagrangian may be chosen as any quantity which is desired to be minimized as the system evolves over the optimal trajectory. The equality constraints force the optimal trajectory to obey the given dynamic equations [12].

The Hamiltonian, which is a scalar function, is defined as:

$$H = \phi(\boldsymbol{x}(t), \boldsymbol{u}(t), t) + \boldsymbol{\lambda}(t)^T \boldsymbol{f}(\boldsymbol{x}(t), \boldsymbol{u}(t), t) \tag{1.10}$$

Then, substituting the Hamiltonian back into equation 1.9, the cost function becomes:

$$J = \int_{t_0}^{t_f} H(\boldsymbol{x}(t), \boldsymbol{u}(t), t) - \boldsymbol{\lambda}(t)^T \dot{\boldsymbol{x}}(t)\, dt \tag{1.11}$$

The calculus of variations can be used to derive the necessary conditions for a trajectory to be optimal under a particular Lagrangian. In the calculus of variations approach, the first variation of the cost function must vanish to zero at the optimal trajectory [13]. By differentiation under the integral sign, the first variation of the cost function J is [12]:

$$\delta J = \int_{t_0}^{t_f} \left[H_x^T \delta x + H_u^T \delta u - \lambda^T \delta \dot{x} + (H_\lambda - \dot{x})^T \delta \lambda \right] dt \tag{1.12}$$

The variation in $\dot{x}$ can be eliminated via integration by parts as follows [12]:

$$\int_{t_0}^{t_f} -\lambda^T \delta \dot{x} \, dt = \int_{t_0}^{t_f} \dot{\lambda}^T \delta x \, dt + \text{boundary terms} \tag{1.13}$$

Substituting 1.13 back into equation 1.12 produces the following result:

$$\begin{aligned} \delta J &= \int_{t_0}^{t_f} \left[H_x^T \delta x + H_u^T \delta u + \dot{\lambda}^T \delta x + (H_\lambda - \dot{x})^T \delta \lambda \right] dt \\ &= \int_{t_0}^{t_f} \left[(H_x^T + \dot{\lambda}^T) \delta x + (H_\lambda - \dot{x})^T \delta \lambda + H_u^T \delta u \right] dt \end{aligned} \tag{1.14}$$

The necessary condition for an optimal trajectory is that the first variation δJ must vanish to 0. This must be true for any arbitrary variations of δx, δu, and $\delta \lambda$ [13]. Thus each term in the integrand above must vanish to zero which yields the following conditions for an optimal trajectory:

$$H_x + \dot{\lambda} = 0 \tag{1.15}$$

$$H_\lambda - \dot{x} = 0 \tag{1.16}$$

$$H_u = 0 \tag{1.17}$$

or as they are more commonly written:

$$\partial_\lambda H = \dot{x} \tag{1.18}$$

$$\partial_x H = -\dot{\lambda} \tag{1.19}$$

$$\partial_u H = 0 \tag{1.20}$$

Equations 1.18 are known as the state equations, equation 1.19 are called the co-state equations, and equation 1.20 is the stationary condition.

1.4.2 Pontryagin's Minimum Principle

The Pontryagin Minimum Principal (PMP) is a necessary condition that a control function must satisfy to be a candidate for optimality. The principle states that the optimal control function is the one that both satisfies the boundary conditions on the problem and which minimizes the Hamiltonian.

Let $u(t)$ be any admissible control, let Ω be the family of all admissible control laws, and let $u^*(t)$ be the optimal control function in Ω for a given problem. An admissible control is defined as a control that evolves the system of states and co-states from the initial conditions to the final conditions. Let $x(t)$ be the set of states and let $\lambda(t)$ be the set of co-states corresponding to an admissible control function $u(t)$ which satisfy the boundary conditions of the problem. Let $x^*(t)$ and $\lambda^*(t)$ be the optimal states and co-states corresponding to the optimal control law $u^*(t)$.

Pontryagin's Minimum Principle states that the value of the Hamiltonian has an absolute minimum at the optimal control law [14], i.e.

$$\min_{u\in\Omega} H(x(t),\lambda(t),u(t)) = H(x^*(t),\lambda^*(t),u^*(t)) \tag{1.21}$$

or, equivalently

$$H(x^*(t),\lambda^*(t),u^*(t)) \leq H(x(t),\lambda(t),u(t)) \tag{1.22}$$

for all $u(t)$ in Ω.

Pontryagin's Minimum Principle also states that the value of the Hamiltonian of the optimal control function is constant across time [14], i.e.

$$H(x^*(t), \lambda^*(t), u^*(t)) = H_0 \tag{1.23}$$

1.4.3 Singular Arcs

When the Hamiltonian contains terms where the control variable is at least quadratic, the stationary condition 1.20 will contain a control value term that can be solved in terms of the states and co-states. In general, the control law derived from the stationary condition for these kinds of problems will depend on both the states and co-states. Finding the optimal trajectory for this class of problems involves picking the correct boundary conditions for the states and co-states and evolving the system along the optimal control law. These boundary conditions are called transversality conditions.

The transversality conditions are derived from the boundary terms which were ignored in the derivation in section 1.4.1. Typically the boundary conditions for the state equations occur at the beginning of the trajectory, and the boundary conditions for the co-state equations occur at the end of the trajectory.

Special consideration must be taken when the Hamiltonian function is linear with respect to the control variable, or equivalently if $H_{uu} = 0$. In this case, the first derivative of the Hamiltonian with respect to the control variable H_u will be independent of the control variable u.

When this happens, the stationary equation 1.20 is independent of the control variable u. This implies that the Hamiltonian is not sensitive to the control variable while the system is on the optimal trajectory. This means that it is impossible to directly minimize the Hamiltonian as required by Pontryagin's Minimum Principle by choosing the control variable. In this case, the optimal trajectory is said to lie on a singular arc.

In some cases, an optimal control law can still be found when the optimal trajectory lies on a singular arc. Typically the procedure for finding the optimal control law involves differentiating the stationary condition and then algebraically manipulating the system of equations formed by the state, co-state, stationary, and stationary derivative equations. An example of a derivation is given below in 2.2.

1.4.4 Necessary Conditions

The stationary condition is a necessary condition for the trajectory to be optimal. To verify that the Lagrangian is minimized, as opposed to a maximum or saddle point, a second-order test must be conducted.

In general, the second-order condition for optimality is:

$$H_{uu}(x(t), \lambda(t), u(t), t) \geq 0 \tag{1.24}$$

The above is called the Legendre-Clebsch condition [15].

There is a strengthened version of the Legendre-Clebsch test as follows:

$$H_{uu}(x(t), \lambda(t), u(t), t) \geq \alpha \tag{1.25}$$

for some positive α. If the strengthened Legendre-Clebsch test holds, it guarantees that u(t) is a local minimizer of the Hamiltonian almost everywhere on the trajectory [15].

1.4.5 Generalized Legendre-Clebsch Conditions for Singular Arcs

When the system stationary equation forms a singular arc, the Legendre-Clebsch test above is not useful. This is because when the system is singular, in all cases $H_{uu} = 0$.

Kelly et al. showed that there is a generalized Legendre-Clebsch test that can be used when an optimal control solution lies on a singular arc [16]. The generalized test is as follows:

$$\frac{\partial}{\partial_u}\left[\frac{d^2}{dt^2}H_u(x(t),\lambda(t),u(t))\right] \leq 0 \tag{1.26}$$

A more generalized version of this test is given in Bryson and Ho when systems of equations must be considered, and is reproduced below [17]:

$$(-1)^k\frac{\partial}{\partial u}\left[\left(\frac{d}{dt}\right)^{2k}H_u\right] \geq 0, \quad k = 0, 1, 2, \ldots. \tag{1.27}$$

It can be seen that the test in equation 1.26 is a special case of this more general result by inspection. In general, a term will fall out of the test which contains the control law through an even number of differentiations with respect to time [17].

The general procedure behind this test is to first take the time derivative of the Hamiltonian with respect to the control function u. This will cause several partial derivatives to appear in the expression. These can be eliminated by substituting the state and co-state equations into the expression. A second derivative is then taken, and the same procedure is followed. At this point, at least one of the terms in the expression will include the control variable. When the expression is differentiated with respect to the control variable for the final time, these terms will form the test for the generalized Legendre-Clebsch condition. An example of the specific problem studied by this thesis is worked through in the section 2.3.

Chapter 2

Optimal Control of a General Class of Non-linear WECs

In this chapter, the general solution for the optimal control law which maximizes the power generated by a WEC is presented.

Section 2.1 builds up the class of non-linear dynamic models which are considered for optimal control. First, a linear model will be discussed. Then, a generalization of this model which admits a certain useful class of non-linear forces will be defined.

This generalized model will be used in the derivation of an optimal control law in section 2.2. The Legendre-Clebsch conditions will then be worked out for this optimal control law in section 2.3, showing that a singular arc is a candidate for maximum power generation.

The relationship between the general optimal control law and complex conjugate control will be explored in section 2.4.

The control law will be applied to the linear model in section 2.5. Numerical analysis will be performed to show the behavior of the system both on and off the singular arc. It will be shown that an infinite number of singular arcs exist, only one of which maximizes the power generated. The construction of the family of singular arcs will be discussed. The optimal singular arc can be found through numerical optimization.

Finally, the control law will be applied to an hourglass buoy in section 2.6. Numerical simulation will be performed to show that the system is operating on a singular arc. Numerical optimization methods will be used to search for the optimal singular arc.

2.1 Dynamic System Model

A free-body diagram for a simple linear wave energy converter buoy in heave is shown in figure 2.1.

Let ζ be the position of the buoy in the heave direction. Then the dynamic system model for the buoy is given by equation 2.1. It is found by summing the forces in the

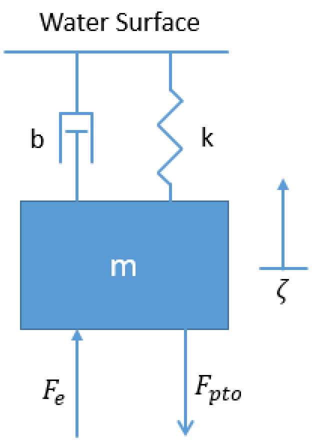

Figure 2.1: Free body diagram of simple dynamic model

free-body diagram.

$$m\ddot{\zeta} + b\dot{\zeta} + k\zeta = F_e(t) - F_{pto} \tag{2.1}$$

where m is the mass of the buoy, c is the damping coefficient, k is the spring constant, F_e is the excitation force from the waves impacting the buoy, and F_{pto} is the force applied to the buoy by the power take-off. Waves are introduced into the model through the excitation force F_e.

The total energy extracted from this system can be written as:

$$E = \int_0^{t_f} F_{pto}\,\dot{\zeta}\,dt \tag{2.2}$$

where t_f is the time horizon to optimize over. A quick dimensional analysis verifies the above equation is physically correct. The dimensions of the integrand are $\left(F_{pto}\ [\mathrm{N}]\right)\left(\dot{\zeta}\ [\frac{\mathrm{m}}{\mathrm{s}}]\right) = [\mathrm{Watts}]$. The integral of [Watts] with respect to time is [Joules] of energy.

An optimal control force that can be applied to this simple buoy model from the power take-off and which maximizes the extracted energy from the model is found in Zou et al and will be re-derived in section 2.5 [1].

One shortcoming of the simplified model 2.1 is that it cannot capture realistic non-linear hydrostatic and hydrodynamic force interactions between a buoy and the water surface. For instance, it may be desirable to analyze a model which contains Freude-Krylov hydrostatic or hydrodynamic forces.

This thesis considers dynamic models with any non-linear force which may be written as a function of buoy position ζ and time t. This class of functions allows for the modeling of many interesting non-linear spring-like forces. These spring-like forces are usually some non-linear function of the distance between the water surface and the buoy position. It is necessary to include time as a dependency of the force function to allow the water surface to evolve. A free-body diagram for models of this type is shown in figure 2.2.

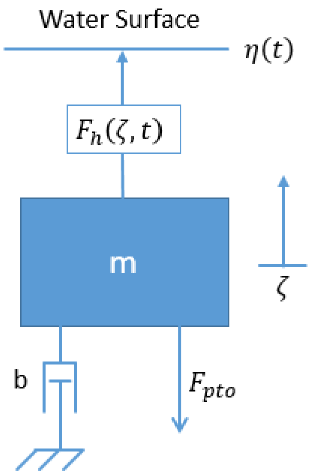

Figure 2.2: Free body diagram of simple dynamic model

A dynamic model corresponding to the free-body diagram in figure 2.2 with a generalized force term is given in equation 2.3.

$$m\ddot{\zeta} + b\dot{\zeta} = F_h(\zeta, t) - F_{pto} \tag{2.3}$$

Note that in this model, the water surface is represented as $\eta(t)$ which is some arbitrary function of time. Typically the non-linear force on the buoy is given as a function $\eta(t)$ and ζ - e.g. the force function usually looks like $F_h(\zeta, \eta(t))$. Note that this is a special case of the class of the family of force functions $F_h(\zeta, t)$ which are considered.

It is important to note that equation 2.3 is a strict generalization of equation 2.1 where

$$F_h(\zeta, t) = -k\zeta + F_e(t) \tag{2.4}$$

Examples of realistic hydrostatic and hydrodynamic models which can be represented by $F_h(\zeta, t)$ will be considered later in this thesis.

2.2 General Optimal Control Solution

A general control function is derived which will keep any model in the class of dynamic systems described by equation 2.3 on the optimal singular arc. While the system is on the optimal arc, the amount of power extracted from the device will be maximized.

First, the dynamic model in equation 2.3 is transformed into state space. Let $u = F_{pto}$ represent the control force in the model. The following state assignments are used:

$$x_1 = \zeta \tag{2.5}$$

$$x_2 = \dot{\zeta} \tag{2.6}$$

$$x_3 = t \tag{2.7}$$

Time is included as a state because the system is non-autonomous (i.e. the non-linear force function $F_h(\zeta, t)$ can depend on time). This is necessary for allowing the location of the surface of the water to evolve with time.

The transformation into state space is given below:

$$\dot{x_1} = x_2 \tag{2.8}$$

$$m\,\dot{x_2} = F_h(x_1, x_3) - u - b\,x_2 \tag{2.9}$$

$$\dot{x_3} = 1 \tag{2.10}$$

The Lagrangian to optimize over will be defined as the negative of the energy extracted from the device, given below.

$$\phi(\boldsymbol{x}, u) = -u\,x_2\,dt \tag{2.11}$$

The negative sign is included in the Lagrangian as the optimization problem is set up as a minimization problem. Minimizing the negative of the energy extracted is equivalent to maximizing the energy extracted. It is interesting to note that the same control law will be derived regardless if this negative sign is included or not. However, the negative sign is important when performing the Legendre-Clebsch second-order tests.

It will be assumed that there are no limits on the control force which can be applied in this problem formulation. This is a reasonable assumption as the power take-off needs to be capable of producing the force required to keep the system on the singular arc. If it is not, the system will leave the singular arc, and optimal power extraction will not be achieved.

Let $\boldsymbol{\lambda}$ be the vector of co-states, and let $\boldsymbol{f}$ be the vector of state equations. Then the Hamiltonian for the system can then be defined as follows:

$$\begin{aligned} H &= \phi(\boldsymbol{x}, u) + \boldsymbol{\lambda}^T \boldsymbol{f}(\boldsymbol{x}, u, t) \\ &= -u\,x_2 + \lambda_1\,x_2 + \frac{\lambda_2}{m}\,\big[F_h(x_1, x_3) - u - b\,x_2\big] + \lambda_3 \end{aligned} \tag{2.12}$$

The state equations which can be re-computed from the Euler-Lagrange equation 1.18 take the same form as in equations 2.8, 2.9, and 2.10. The co-state equations can be computed from the Euler-Lagrange equation 1.19 as follows:

$$-\dot{\lambda}_1 = \frac{\lambda_2}{m}\,\partial_{x_1} F_h(x_1, x_3) \tag{2.13}$$

$$-\dot{\lambda}_2 = -u + \lambda_1 - \frac{b}{m}\lambda_2 \tag{2.14}$$

$$-\dot{\lambda}_3 = \frac{\lambda_2}{m}\,\partial_{x_3} F_h(x_1, x_3) \tag{2.15}$$

The stationary condition (computed from equation 1.20) is as follows:

$$-x_2 - \frac{\lambda_2}{m} = 0 \tag{2.16}$$

The state, co-state, and constraint equations can be solved algebraically to derive a closed-form solution for the control force u in terms of the states and the excitation force. The derivation is shown below.

The first step in the derivation is to find algebraic relations for λ_1 and λ_2. A constraint for λ_2 can be solved from equation 2.16 when the stationary condition holds (i.e. the system is on a singular arc).

$$\boxed{\lambda_2 = -m x_2} \tag{2.17}$$

The above can be differentiated to produce:

$$\dot{\lambda_2} = -m\dot{x_2} \tag{2.18}$$

Then equation 2.18 is combined with equation 2.14 to form the following:

$$m\dot{x_2} = -u + \lambda_1 - \frac{b}{m}\lambda_2 \tag{2.19}$$

Equation 2.17 is used to eliminate λ_2 from the above.

$$m\dot{x_2} = -u + \lambda_1 + b\,x_2 \tag{2.20}$$

The state equation 2.9 is used to eliminate $\dot{x_2}$ from the above.

$$F_h(x_1, x_3) - u - bx_2 = -u + \lambda_1 + b\,x_2 \tag{2.21}$$

The above result can be simplified to find an algebraic relation for λ_1 when the stationary condition holds.

$$\boxed{\lambda_1 = F_h(x_1, x_3) - 2b\, x_2} \tag{2.22}$$

The two algebraic constraints for λ_1 and λ_2 can be combined with the state and co-state equations to find an algebraic solution for u. The above result can be differentiated with respect to time as shown below:

$$\dot{\lambda_1} = \dot{x_1}\, \partial_{x_1} F_h(x_1, x_3) + \dot{x_3}\, \partial_{x_3} F_h(x_1, x_3) - 2b\, \dot{x_2} \tag{2.23}$$

The co-state equation 2.13 can be substituted into the above to eliminate $\dot{\lambda_1}$.

$$-\frac{\lambda_2}{m} \partial_{x_1} F_h(x1, x3) = \dot{x_1} \partial_{x_1} F_h(x_1, x_3) + \dot{x_3} \partial_{x_3} F_h(x_1, x_3) - 2b\, \dot{x_2} \tag{2.24}$$

Equation 2.17 can be used to eliminate λ_2 from the equation above. Equation 2.8 can be used to eliminate $\dot{x_1}$, equation 2.9 can be used to eliminate $\dot{x_2}$, and equation 2.10 can be used to eliminate $\dot{x_3}$.

$$x_2 \partial_{x_1} F_h(x1, x3) = x_2 \partial_{x_1} F_h(x_1, x_3) + \partial_{x_3} F_h(x_1, x_3) - \frac{2c}{m}(F_h(x_1, x_3) - u - b\, x_2) \tag{2.25}$$

The above equation can be simplified to yield the following:

$$u = F_h(x_1, x_3) - b\,x_2 - \frac{m}{2b}\partial_{x_3} F_h(x_1, x_3) \tag{2.26}$$

The state definitions can be substituted into equation 2.26 to yield the general optimal control law when the system is on the singular arc.

$$\boxed{u_{sa} = F_h(\zeta, T) - b\,\dot{\zeta} - \frac{m}{2b}\,\partial_T\, F_h(\zeta, T)} \tag{2.27}$$

This optimal control law is broadly applicable under a wide variety of buoy models and is the main result of this thesis.

Once the optimal control law is known, the third co-state constraint equation can be found. The co-state constraint equations show how the co-states will evolve if the stationary condition is met, i.e. the system is on a singular arc.

The third co-state constraint can be found by the following procedure. First, an observation must be made that the Hamiltonian will be some constant value when the system is on an optimal arc, which comes from Pontryagin's Minimum Principle. Because λ_3 appears alone at the end of the Hamiltonian, it can be expressed as $\lambda_3 =$ (some expression forcing the Hamiltonian to be constant) $+\ C$ without loss of generality. This means that for this particular system, the value of the Hamiltonian constant can be chosen by picking C.

From the above observation, let

$$H = C \tag{2.28}$$

Then by substituting the optimal control law from equation 2.27 as well as the previous co-state constraints from equation 2.22 and 2.17 into the above equation, the following expression is found:

$$-bv^2 + \lambda_3 = C. \tag{2.29}$$

Arbitrarily choose $C = 0$, then, when the system is on the singular arc,

$$\boxed{\lambda_3 = b\,v^2} \tag{2.30}$$

2.3 Legendre-Clebsch Necessary Conditions

The generalized Legendre-Clebsch test is followed for the singular arc found in section 2.2. The generalized test, which is found in equation 1.26 is re-written for convenience:

$$\frac{\partial}{\partial_u}\left[\frac{d^2}{dt^2}H_u(x(t),\lambda(t),u(t))\right]\leq 0 \tag{2.31}$$

The derivative of the Hamiltonian with respect to the control variable u is below:

$$H_u = -x_2 - \frac{\lambda_2}{m} \tag{2.32}$$

Note that this quantity is used to compute the stationary condition in equation 2.16.

The first time derivative of H_u is:

$$\frac{d}{dt}H_u = -\dot{x_2} - \frac{\dot{\lambda_2}}{m} \tag{2.33}$$

Equation 2.9 and equation 2.13 are substituted into the above to yield:

$$
\begin{aligned}
\frac{d}{dt}H_u &= -\frac{F_{nl}(\zeta,T) - u - bv}{m} - \frac{u - \lambda_1 + \frac{b}{m}\lambda_2}{m} \\
&= -\frac{F_{nl}(\zeta,T)}{m} + \frac{bv}{m} + \frac{\lambda_1}{m} - \frac{b\lambda_2}{m^2}
\end{aligned}
\tag{2.34}
$$

The second time derivative is taken of the above:

$$
\begin{aligned}
\frac{d^2}{dt^2}H_u = &-\frac{\dot{\zeta}\,\partial_\zeta\, F_{nl}(\zeta,T)}{m} - \frac{\dot{T}\,\partial_T\, F_{nl}(\zeta,T)}{m} \\
&+ \frac{b\dot{v}}{m} + \frac{\dot{\lambda}_1}{m} - \frac{b\dot{\lambda}_2}{m^2}
\end{aligned}
\tag{2.35}
$$

State and co-state equations are substituted into the above to yield the following:

$$
\begin{aligned}
\frac{d^2}{dt^2}H_u = &-\frac{\dot{\zeta}\,\partial_\zeta\, F_{nl}(\zeta,T)}{m} + \frac{\partial_T\, F_{nl}(\zeta,T)}{m} \\
&+ \frac{bF_{nl}(\zeta,T)}{m^2} - \frac{2bu}{m^2} - \frac{b^2v}{m^2} \\
&- \frac{\lambda_2\partial_\zeta F_{nl}(\zeta,T)}{m^2} \\
&+ \frac{b\lambda_1}{m^2} - \frac{b^2\lambda_2}{m^3}
\end{aligned}
\tag{2.36}
$$

Only one term in the above contains the control variable u, so when the derivative of the above with respect to u is taken, only one term survives.

$$\partial_u \frac{d^2}{dt^2} H_u = -\frac{2b}{m^2} \tag{2.37}$$

The second-order test can then be performed as follows:

$$\boxed{\left(\partial_u \frac{d^2}{dt^2} H_u = -\frac{2b}{m^2}\right) \leq 0} \tag{2.38}$$

The generalized Legendre-Clebsch test always passes because the mass m and damping value b must be positive real values.

2.4 Relationship Between Optimal Solution and Conjugate Control

Zou et al. compared the above optimal control solution for the linear wave energy converters to complex conjugate control through simulation [1]. In this section, the relationship between the two is developed analytically. First, the main result from complex conjugate control is derived [10]. Finally, it is shown that this result is a special case of the general optimal control solution.

2.4.1 Derivation of Complex Conjugate Control

The conjugate control optimal constraint for a linear system in regular waves is derived below.

First, the linear dynamic equation is given in equation 2.39. ζ is the position of the buoy, f_e is the excitation force, and f_L is the force applied by the power take-off (also called the load force).

$$m\ddot{\zeta} + b\dot{\zeta} + k\zeta = f_e + f_L \tag{2.39}$$

Because the system, the excitation, and load forces are periodic, the system can be analyzed in the Laplace domain. The substitution $s = i\omega$ is made to study the frequency response of the system.

$$(s^2 m + sb + k)Z = F_e + F_L \tag{2.40}$$

$$(-m\omega^2 + bi\omega + k)Z = F_e + F_L \tag{2.41}$$

The analysis below will be more concerned with the velocity than the position of the system, so a new variable V is defined as the velocity of the system. The position and velocity are related through a derivative, so $sZ = V$. Again, the substitution $s = i\omega$ is made.

$$(i\omega)Z = V \quad \Rightarrow \quad Z = -\frac{i}{\omega}V \tag{2.42}$$

The load force is defined to be a constant dissipative/resistive load which must have the following form, where d is a positive real number:

$$F_L = -d(V) \tag{2.43}$$

Substituting equation 2.42 and the form of the load force from equation 2.43 back into equation 2.41 yields the following equation:

$$(i\omega m + (b + d) - \frac{i}{\omega}k)V = F_e \tag{2.44}$$

The above can be solved for velocity to yield the following expression:

$$V = \frac{F_e}{i\omega m + (b + d) - \frac{i}{\omega}k} \tag{2.45}$$

The idea of complex conjugate control is to force the system to operate at resonance. This can be seen to be ideal from inspection of the following argument. When the reactive terms in the system equation are forced to zero, then a given excitation force will translate into the largest possible dissipative force, which is desirable for power extraction. When the system is operating at resonance, the following constraint must hold:

$$i\omega m - \frac{i}{\omega}k = 0 \tag{2.46}$$

When the above resonance constraint is substituted into equation 2.45, the following result for the velocity of the system is found:

$$V = \frac{F_e}{b + d} \tag{2.47}$$

Maximization of the extracted power using calculus will now be performed to find the optimal value for d. The power extracted is defined as the negative of the product of the velocity and the load force applied to the system.

$$P = -V\,F_L \quad \Rightarrow \quad P = V^2\,d \tag{2.48}$$

Substituting the above back into equation 2.47 yields the following result for the extracted power:

$$P = -\frac{d\,{F_e}^2}{(b+d)^2} \tag{2.49}$$

The above power result can be maximized by setting the derivative with respect to the free parameter d to zero.

$$\partial_d P = 0 \quad \Rightarrow \quad \frac{b-d}{b+d}\,Fe = 0 \tag{2.50}$$

Equation 2.50 result can be solved to find the optimal value of d.

$$b - d = 0 \quad \Rightarrow \quad b = d \tag{2.51}$$

The power transfer out of the system is maximized when the impedance of the power take-off is matched with the impedance of the buoy. The above result can be substituted back into equation 2.47 to find the optimal constraint on the velocity for complex conjugate control in the frequency domain.

$$V = \frac{F_e}{2b} \tag{2.52}$$

Finally, the result can be translated out of the frequency domain and back into the time domain to yield the general constraint on the velocity of the system for optimal power transfer. This constraint is valid as long as all excitation forces are periodic, i.e. the frequency domain analysis used above holds.

$$\boxed{\dot{\zeta} = \frac{f_e}{2b}} \tag{2.53}$$

The above is the well-known main result from complex conjugate control [10].

2.4.2 Relationship with Optimal Control

The main complex conjugate control result can be recreated from the optimal control result for a linear system. The dynamic equation for a linear system is written below:

$$m\,\ddot{\zeta} + c\,\dot{\zeta} + k\,\zeta = F_e - u \tag{2.54}$$

The optimal control law for a linear system is shown below:

$$u = F_e - c\,\dot{\zeta} - k\,\zeta - \frac{m}{2b}\dot{F}e \tag{2.55}$$

Substituting equation 2.55 into equation 2.54 yields the following equation:

$$m\,\ddot{\zeta} + c\,\dot{\zeta} + k\,\zeta = Fe - \left(Fe - c\,\dot{\zeta} - k\,\zeta - \frac{m}{2b}\dot{F}e\right) \tag{2.56}$$

All terms but the $m\ddot{\zeta}$ term and the $\frac{m}{2b}\dot{F}e$ term cancel. Therefore, the above can be simplified into the following:

$$\ddot{\zeta} = \frac{\dot{F}_e}{2b} \tag{2.57}$$

Taking the anti-derivative of the above equation yields the following:

$$\dot{\zeta} = \frac{F_e}{2b} + C \tag{2.58}$$

Integrating the above equation again will show that $\zeta = Ct + E + \int_0^t \frac{F_e(\tau)}{2b}\,d\tau$. The buoy position ζ is required to be periodic which means the linear term must vanish and therefore $C = 0$.

$$\boxed{\dot{\zeta} = \frac{Fe}{2b}} \tag{2.59}$$

This is the same result that was obtained through the derivation of complex conjugate control, which means that complex conjugate control is a special case of the optimal control law (when the system is linear and the waves are regular). However, unlike complex conjugate control, the optimal control law developed here is not limited by these assumptions.

2.5 Application to Linear Buoy Model

The general control law is applied to the linear buoy model. The control law derived is the same as what is given in Zou et al [1]. Bang bang control for the linear model is considered, using a derived switching function. Optimal initial conditions are found that lie on the singular arc. Numerical simulation is provided which verifies the performance of the system, both on and off of the singular arc. Finally, it is shown that there are an infinite number of singular arcs and that they can be constructed by changing the position initial condition.

2.5.1 Application of General Control Law to Linear Buoy

The linear model of the system described by the free body diagram 2.1 is shown in equation 2.1 and is re-written below for convenience. T is capitalized to denote that it represents the time state, not the time t. However, as per equation 2.7, the substitution $T(t) = t$ can be made at the appropriate point in the analysis after all the derivatives with respect to T have been taken.

$$m\ddot{\zeta} + c\dot{\zeta} = f(\zeta, T) - u \tag{2.60}$$

The force term for the linear buoy is defined as given below:

$$f(\zeta, T) = -k(\zeta - \eta(T)) \tag{2.61}$$

The generalized control law (equation 2.27) states that both the force as well as the derivative of the force with respect to the time state are needed. The derivative is simply $\partial_T f(\zeta, T) = k\,\dot{\eta}(T)$.

After the derivatives have been taken, the substitution $T = t$ may be made, and the above can be substituted into equation 2.27 to yield the optimal control law for a linear buoy.

$$\boxed{u_{sa} = k\,\eta(t) - k\,x - b\,v - \frac{k\,m}{2b}\,\dot{\eta}(t)} \tag{2.62}$$

The above equation is true for any general wave height $\eta(t)$, however, a periodic forcing function will be applied for the subsequent analysis.

Let a be the amplitude of the wave applied to the buoy from a regular wave field, and let T_w be the period of that regular wave field. Then the excitation force for the buoy in a regular wave field takes the following form:

$$\eta(t) = a\cos\left(\frac{2\pi}{T_w}\,t\right) \tag{2.63}$$

The derivative, as required by the control law, is computed as the following:

$$\dot{\eta}(t) = -a\,\frac{2\pi}{T_w}\sin\left(\frac{2\pi}{T_w}\,t\right) \tag{2.64}$$

Substituting these into the control law for the linear buoy, the following specific optimal control law for the linear model when the system is on the singular arc is calculated below:

$$\boxed{u_{sa}(t) = k\,a\,\cos\left(\frac{2\pi}{T_w}\,t\right) - b\,v(t) - k\,x(t) + \frac{2\pi\,k\,m\,a}{2b\,T_w}\,\sin\left(\frac{2\pi}{T_w}\,t\right)} \tag{2.65}$$

The above holds when the system is on the singular arc. According to the Pontryagin Minimum Principle, when the system is off the singular arc, the maximum available control should be applied to drive the system back to the singular arc. Let γ be the maximum control available. $\zeta = H_u = -v - \frac{\lambda_2}{m}$ forms a switching function that can be used to drive the system to the stationary condition.

$$\boxed{u(t) = \begin{cases} \gamma & \zeta(t) > 0 \\ u_{sa}(t) & \zeta(t) = 0 \\ -\gamma & \zeta(t) < 0 \end{cases}} \tag{2.66}$$

The switching function ζ is awkward to use because it is in terms of the co-state λ_2. The initial conditions for the co-state are not known when the system is not on the singular arc, making the simulation difficult to implement. A different switching function can be derived as follows [1]:

$$\boxed{\zeta(t) = v(t) - \frac{k}{2b}\eta(t)} \tag{2.67}$$

This switching function is found by substituting the optimal control law 2.27 back into the velocity state equation 2.9 which yields the following:

$$\dot{v} = \frac{k}{2b}\dot{\eta}(t) \tag{2.68}$$

The above can be integrated with respect to time, which produces the equation below:

$$v = \frac{k}{2b}\eta(t) + C \tag{2.69}$$

To find C, the state equation 2.5 can be substituted above, and then the system can be integrated to yield the following expression:

$$\dot{x} = \frac{k}{2b}\eta(t) + C \tag{2.70}$$

$$x = D + Ct + \int_0^t k\,\eta(\tau)\,d\tau \tag{2.71}$$

Because only periodic forcing functions are considered, then $C = 0$.

Solving equation 2.69 for C yields the switching function 2.67 (repeated below for clarity).

$$\zeta = C = v(t) - \frac{k}{2b}\eta(t) \tag{2.72}$$

Because the above was found by substituting the optimal control law into the state equation 2.9, when the switching function $\zeta = 0$, the system must be on the singular arc. When $\zeta \neq 0$, the system is off the singular arc and must be driven back.

2.5.2 Optimal Initial Conditions

The optimal initial conditions for the linear buoy can be computed as follows. The state space for the linear system is given below.

$$\dot{x} = v \tag{2.73}$$

$$\dot{v} = \frac{k(\eta(t) - x) - c\,v - u}{m} \tag{2.74}$$

$$\dot{T} = 1 \tag{2.75}$$

For this simple linear model, the state space can be directly solved.

$$x = tD + C + \frac{k\,a\,T_w}{4\pi\,b}\sin\left(\frac{2\pi}{T_w}t + E\right) \tag{2.76}$$

$$v = D + \frac{k\,a}{2b}\cos\left(\frac{2\pi}{T_w}t + E\right) \tag{2.77}$$

$$T = t + E \tag{2.78}$$

The variables C, D, and E are integration constants. The initial condition for the state T is known to be $T(0) = 0$, which forces $E = 0$. The state x must be periodic, which forces $D = 0$. The initial condition C cannot be determined from the information available and must be found by looking for the condition which maximizes the power extraction from the device. The optimal result ends up being $C = 0$. The fact that C is not determinable is indicative of the fact that there are infinitely many singular arcs, but this will be discussed later in the numerical analysis section 2.5.4.

Then the following are the equations of motion for the system.

$$x = \frac{k\,a\,T_w}{4\pi\,b}\sin\left(\frac{2\pi}{T_w}t\right) \tag{2.79}$$

$$v = \frac{k\,a}{2b}\cos\left(\frac{2\pi}{T_w}t\right) \tag{2.80}$$

$$T = t \tag{2.81}$$

The optimal initial conditions can be computed when $t = 0$ as follows:

$$x(0) = 0 \tag{2.82}$$

$$v(0) = \frac{k\,a}{2b} \tag{2.83}$$

$$T(0) = 0 \tag{2.84}$$

2.5.3 Numerical Simulation on Singular Arc

In this section, a numerical simulation is used to verify the performance of the linear system. The numerical values used in the simulation are provided in Table 2.1. These numerical values will also be used in the non-linear simulations in the sections below for a fair comparison.

Table 2.1
Numerical values of quantities used in linear simulations

Quantity	Value	Units	Description
g	9.81	$\mathrm{m/s^2}$	Acceleration due to gravity
ρ	1000	$\mathrm{kg/m^3}$	Density of water
m	109626	kg	Mass of the buoy
b	20000	N s/m	Linear viscous damping coefficient
k	$\pi\,9810$	N/m	Spring force constant
a	0.5	m	Wave height
T_w	11.8502	s	Period of wave field
γ	20000	N	Max available control force

The linear system was modeled starting at the optimal initial conditions. The initial conditions for the states were found using the values described above. The initial values for the co-states were found using the co-state constraints from equations 2.22 and 2.17. The system is simulated at resonance i.e. the wave period was calculated as $T_w = \frac{1}{2\pi}\sqrt{k/m} \approx 11.8502$.

The position and velocity are shown in figure 2.3. Note that the optimal initial condition for the position state is 0, whereas the optimal initial condition for the velocity state is at the max amplitude of the velocity sinusoid.

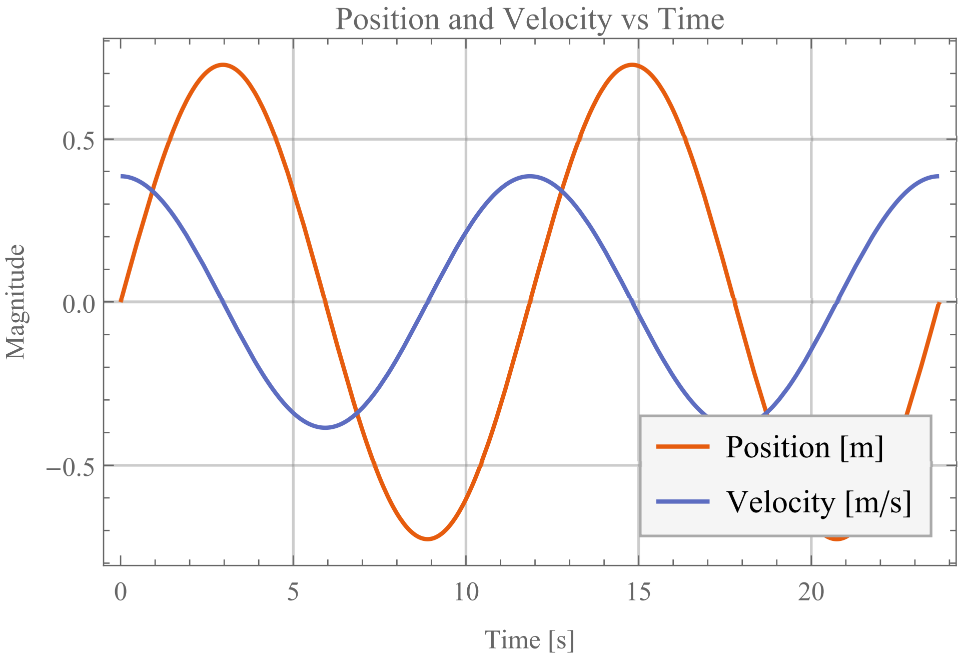

Figure 2.3: Position and velocity of the buoy vs time

Figure 2.4 below shows the velocity and control force overlaid. Note that the control force is in phase with the velocity, yielding maximum power generation.

The velocity and control forces are only perfectly in phase when the frequency of the wave field is equal to the resonant frequency of the linear system. As the wave field frequency moves away from the resonant frequency, the velocity will begin to either lead or lag the control force. This yields a smaller, although still optimal, power generation.

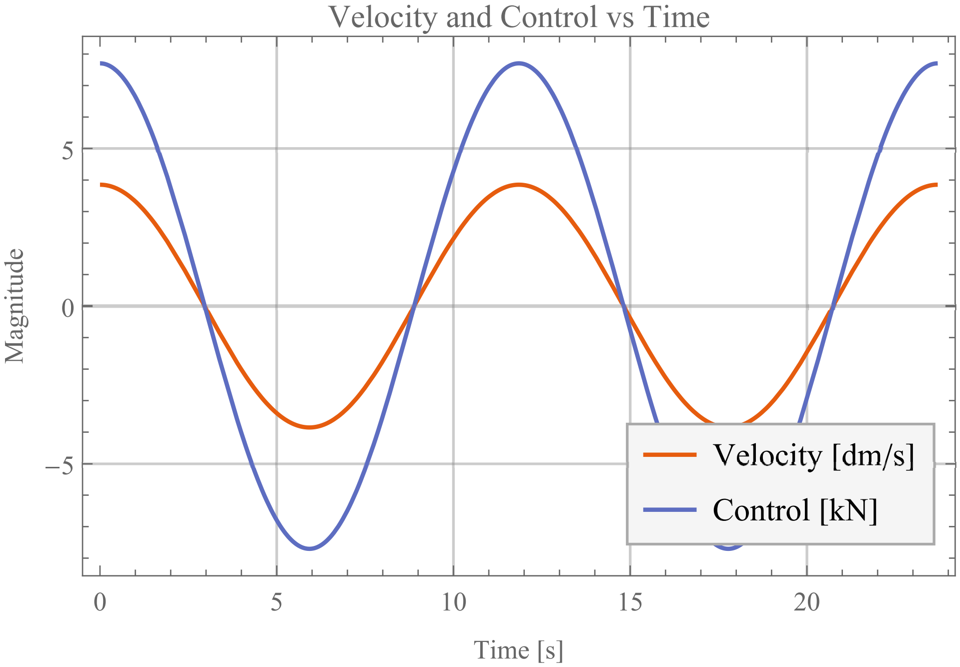

Figure 2.4: Velocity and control force of the buoy vs time. Note that velocity is given in decimeters/second, and control force is given in kilonewtons to make graph scales comparable. The wave field frequency is set at the resonant frequency of the buoy

In Figure 2.5 below, the power transfer out of the device is maximized. Positive power values represent instantaneous power generated by the device. Negative values represent instantaneous power drawn by the device. The blue line shows the average power generated by the device.

At resonance, and starting at optimal initial conditions, power is only generated by the device, and no power is drawn. This represents an optimum power extraction trajectory for the device.

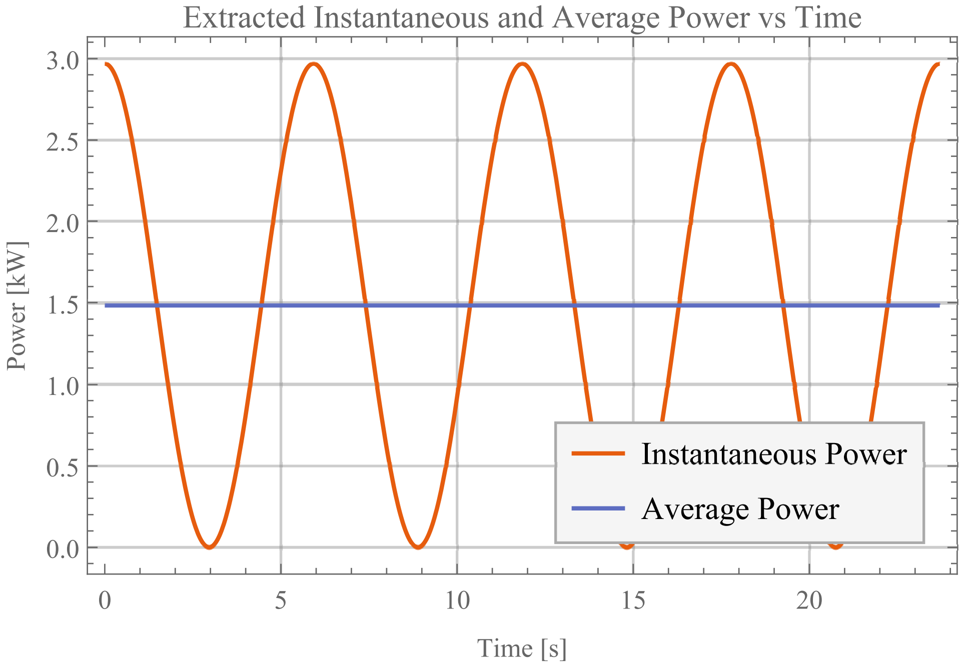

Figure 2.5: Instantaneous and average extracted power from the buoy vs time

At an optimal trajectory, the Hamiltonian should be constant. As seen below in figure 2.6, there are small spikes in the Hamiltonian due to numerical integration error. These spikes were found to decrease as the step size of the integration technique was increased.

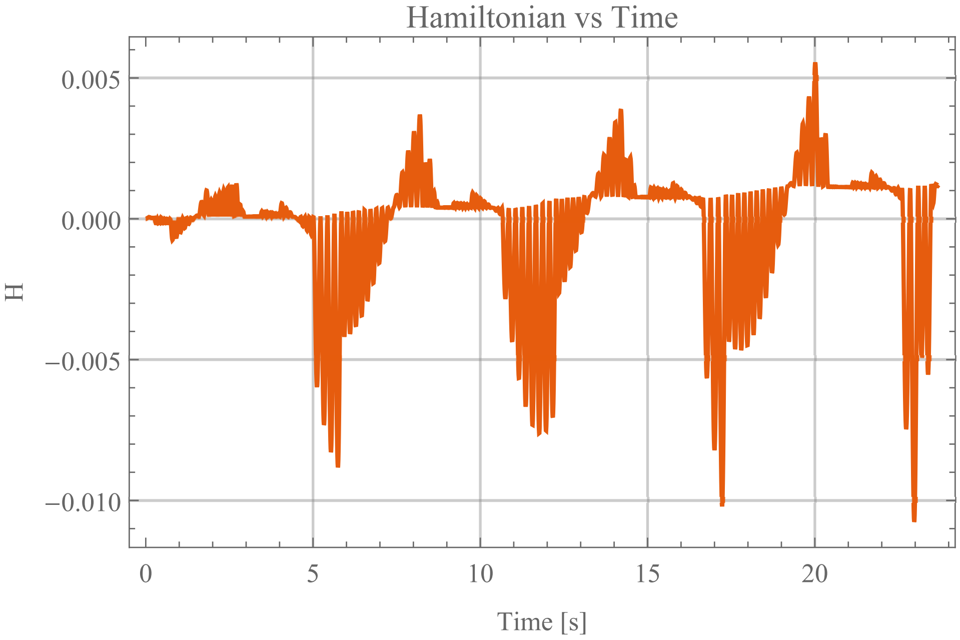

Figure 2.6: Hamiltonian vs time

When on the singular arc, the switching function should be identically equal to 0. Figure 2.7 below shows this to be true. Due to numerical error, there are very slight variations away from 0 once the system is on the singular arc.

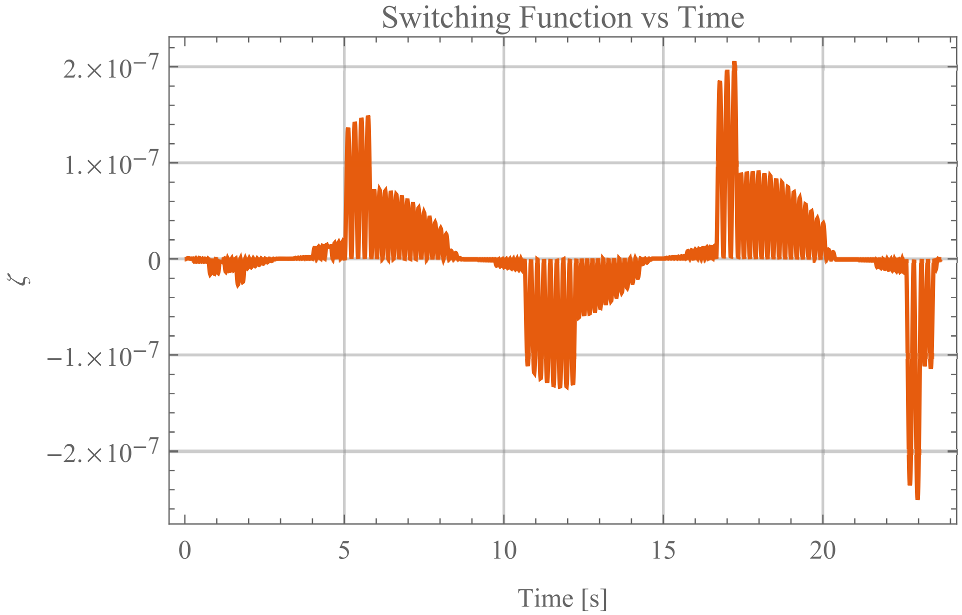

Figure 2.7: Switching function ζ vs time

Figure 2.8 below shows the co-states calculated from the evolved from the co-state equations 2.13, 2.14, and 2.15, and also from the co-state constraint equations 2.22, 2.17, and 2.30. The co-state constraints are derived from the stationary condition in equation 2.16, which is only valid when the system is on the singular arc. Therefore, the fact that the evolved and calculated co-states match is a good check that the system is on the singular arc in this simulation. The fact that the data in the three co-state graphs are line-on-line shows that the simulated system is on a singular arc.

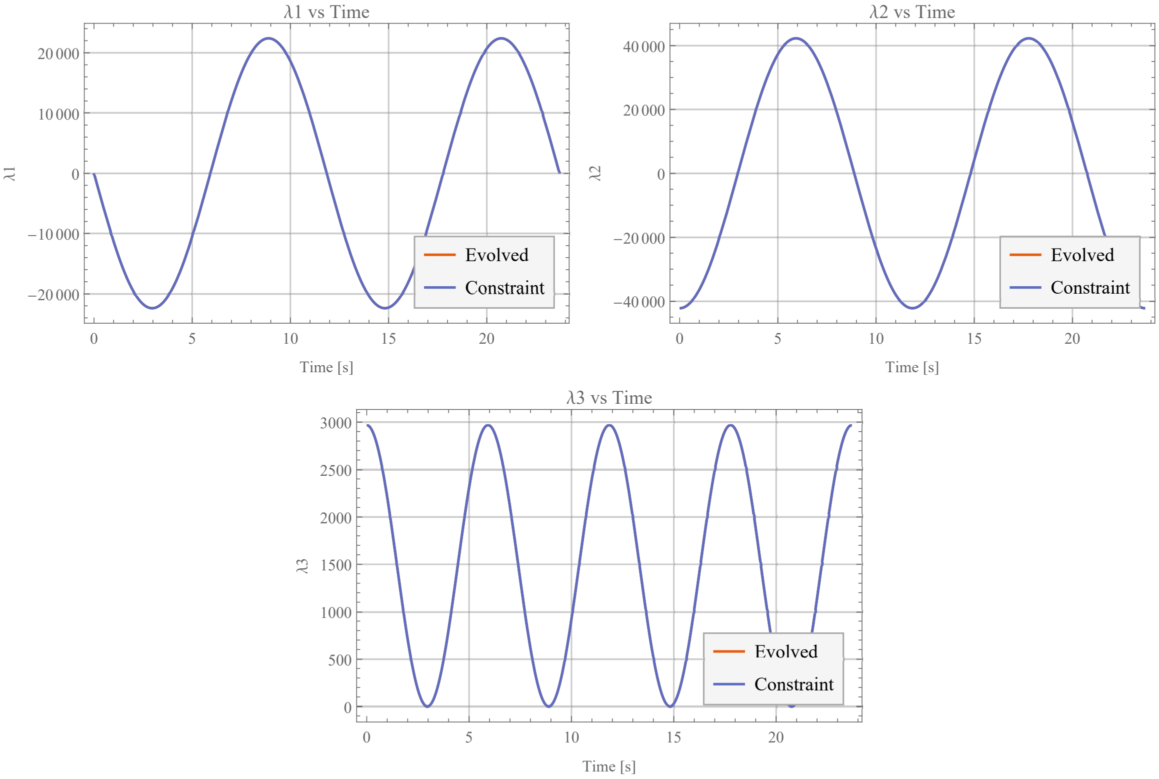

Figure 2.8: Co-state numerically integrated (evolved) from the differential equation and calculated from the singular arc constraint

2.5.4 Numerical Simulation off of Singular Arc

The results from the simulation which was off of the singular arc were derived from starting the system at an initial condition of $(x0, v0) \approx (0.273, 0)$. This initial condition is not on the singular arc.

Figure 2.9 below shows the position vs velocity for the system when the above initial conditions are used. The discontinuity in the velocity around 1.5 seconds arises from the control switching from bang-bang to the singular arc control as the system moves onto the singular arc. The initial choice of the position state will be discussed at the end of this section.

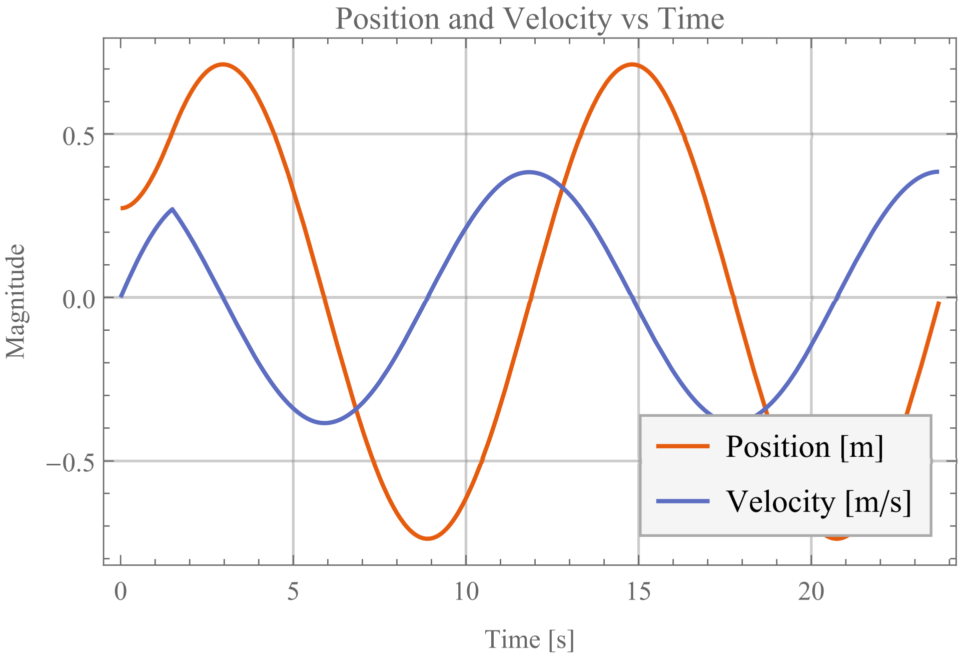

Figure 2.9: Position and velocity vs time with initial conditions $(x0, v0) \approx (0.273, 0)$

Figure 2.10 below shows the control force vs time. For about the first 1.5 seconds, the control is in bang-bang mode because the system is not on the singular arc. After that time, the system arrives on the arc and the singular control law is used. Note that in this simulation, the maximum control force available is $\gamma = 20\,\mathrm{kN}$. This value was chosen as an arbitrary number that was larger than the maximum force required on the singular arc.

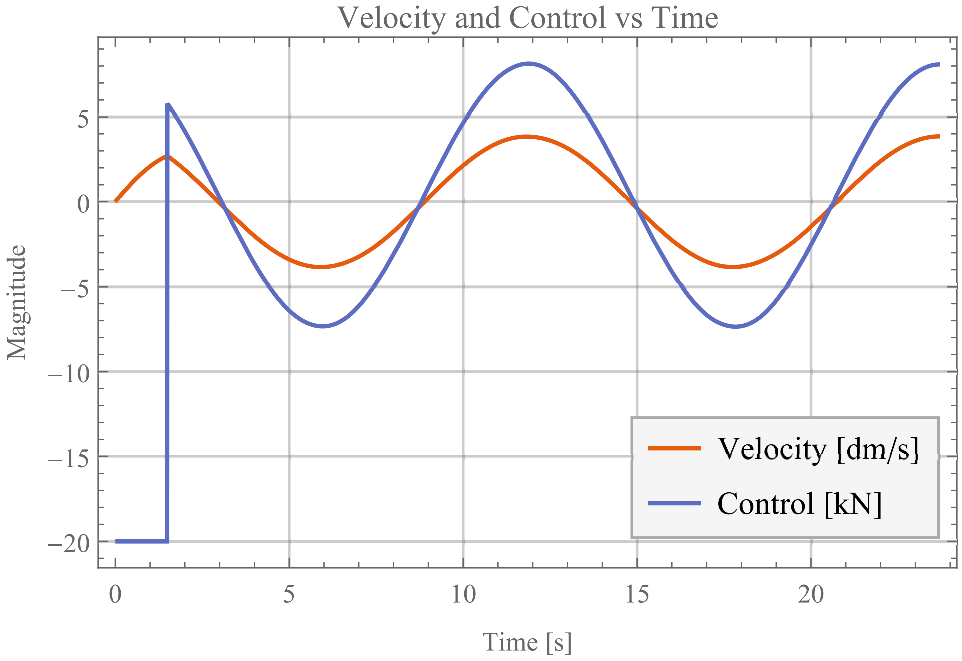

Figure 2.10: Velocity and control force vs time with initial conditions $(x0, v0) \approx (0.273, 0)$. Note that velocity is given in decimeters/second, and control force is given in kilonewtons to make graph scales comparable.

The power generated from this simulation after the system is on the singular arc as shown in figure 2.11 is very similar to the power generated in the previous simulation (shown in figure 2.5). There is a significant power draw in the simulation during the first 1.5 seconds to move the system to the singular arc, maxing out at over 5kW draw. After the system reaches the singular arc, the power generation is very similar to figure 2.5, averaging about 1.5 kW.

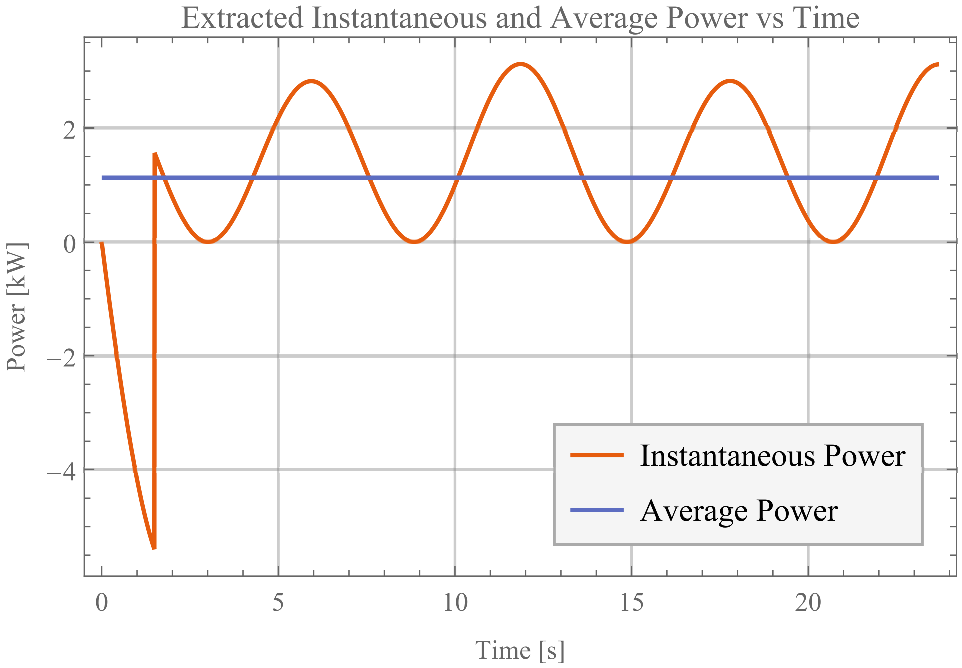

Figure 2.11: Instantaneous and average extracted power from the buoy vs time with initial conditions $(x0, v0) \approx (0.273, 0)$

The switching function is shown in figure 2.12 below. Before about 1.5 seconds, the system is not on the singular arc, and so the switching function is negative. As the system moves to the singular arc, the switching function moves to be almost identically equal to 0.

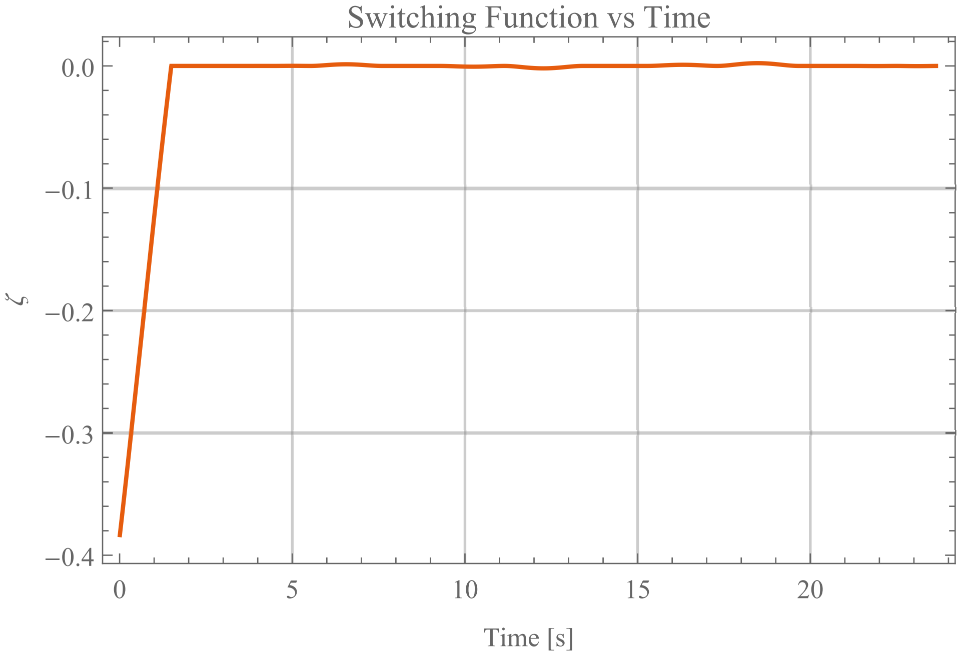

Figure 2.12: Switching function ζ vs time with initial conditions $(x0, v0) \approx (0.273, 0)$

The evolution of the co-states is shown below in figure 2.13. Until about 1.5 seconds, the system is not on the singular arc, and so the evolved co-states from equations 2.13, 2.14, and 2.15 do not match the co-state constraints equations 2.22, 2.17, and 2.30. At about 1.5 seconds, the system is driven to the singular arc. At this point, the evolution of the co-states is known to match the co-state constraint equations. Because the initial conditions of the co-states are not known at the beginning of the simulation but are known when the system lands on the singular arc, the values of the co-states must be updated in the numerical integration routine when the system lands on the singular arc. After the co-states are updated, the full system is allowed to continue to evolve.

In figure 2.13 below, it can be seen that evolved and constraint graphs of λ_1, λ_2, and λ_3 are essentially line-on-line once the system reaches the singular arc. Any discrepancies come from errors in the numerical integration.

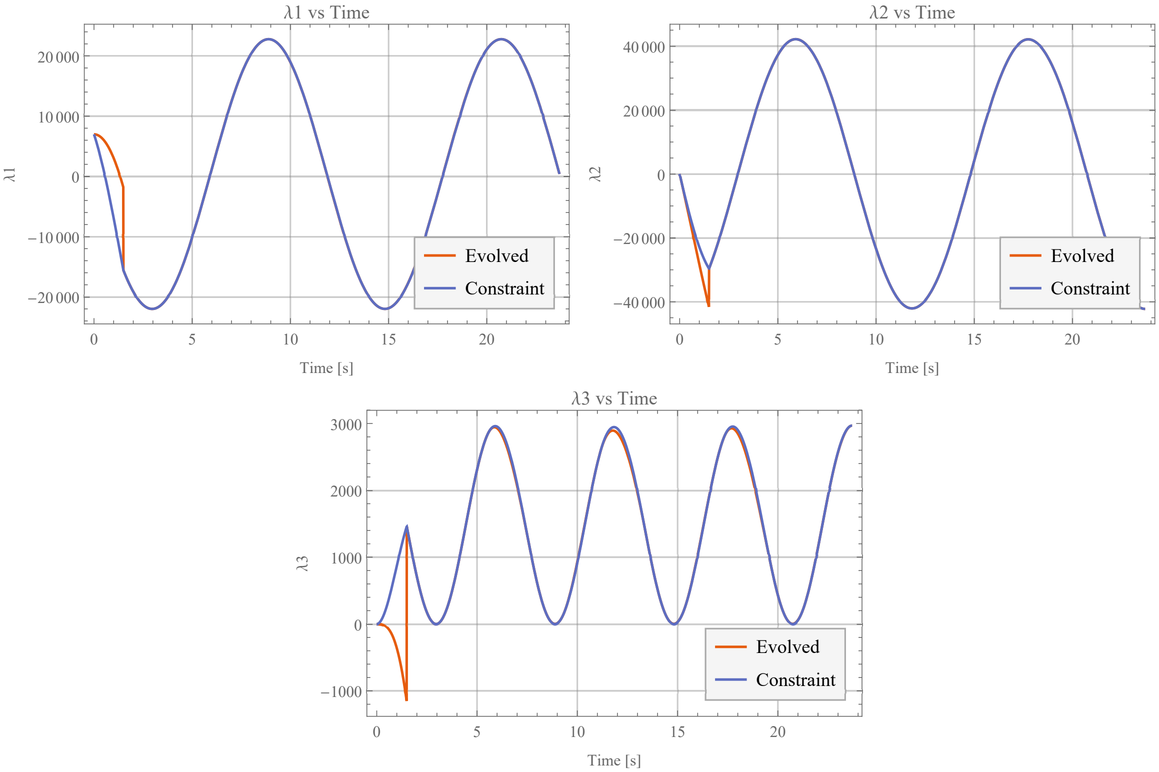

Figure 2.13: Co-state numerically integrated (evolved) from the differential equation and calculated from the singular constraint with initial conditions $(x0, v0) \approx (0.273, 0)$

There are an infinite number of initial conditions which meet the requirements for being a singular arc. This can be seen by integrating the switching function from equation 2.67. Integrating this equation yields $x(t) = E + \frac{1}{2c}\int_0^t f_e(\tau)\,d\tau$, where E is an integration constant, and τ is a dummy integration variable. Like equation 2.67, this equation is valid when the system is on a singular arc. There are no constraints on the integration constant E, and from this, it can be seen that the system is on the singular arc for any initial condition for the position state.

The initial condition for the position state does have a significant effect on the power generation of the system. If the position initial condition is not chosen correctly, the system will oscillate in a lopsided manner, and the amount of average power generated will be reduced. An example of this is shown in the simulations shown below.

For the following simulations, the initial conditions were chosen as $(x0, y0) = (0, 0)$. Note that the $x0$ initial condition is different than the optimal initial condition of about $x0 = 0.273$ used in the simulations above.

It can be seen that unlike in figure 2.9, the system in figure 2.14 below has a lopsided position which has a max value of about 0.5 meters and a min value of about -1.0 meters.

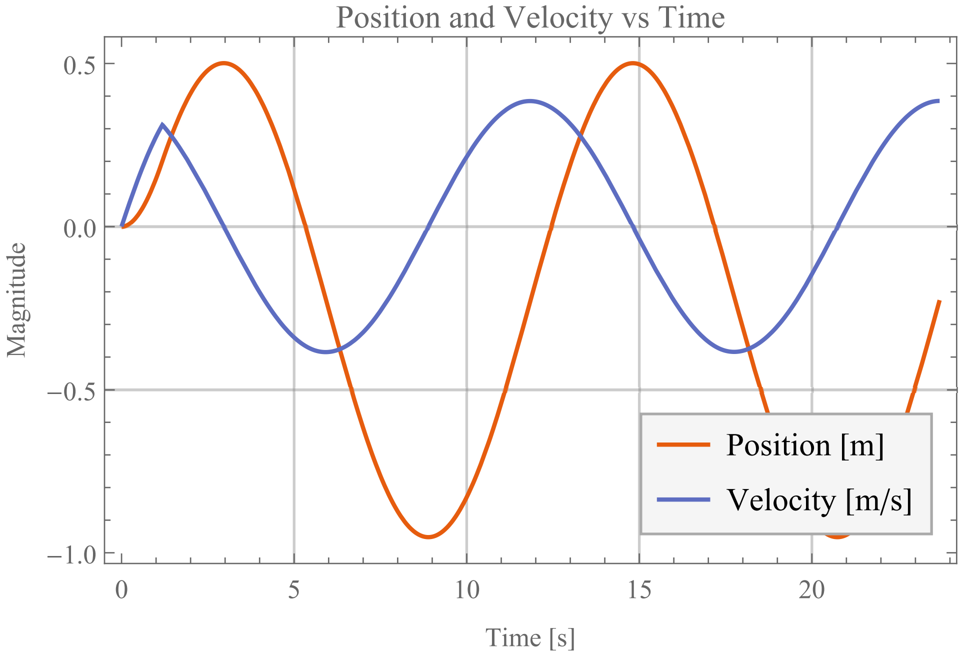

Figure 2.14: Position and velocity vs time with initial conditions $(x0, v0) = (0, 0)$

There is a constant offset in the control function as compared to figure 2.10. The offset is required to drive the position of the system in the lopsided manner shown in the graph above. This additional control effort will reduce the power extracted from the system, even though the system is on a singular arc.

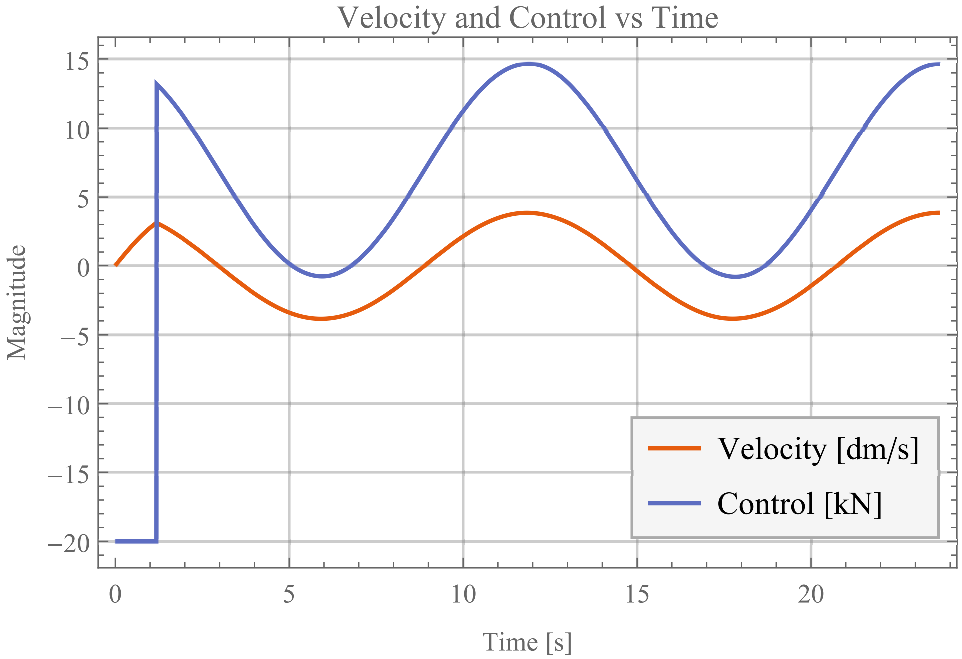

Figure 2.15: Velocity and control force vs time with initial conditions $(x0, v0) = (0, 0)$. Note that velocity is given in decimeters/second, and control force is given in kilonewtons to make graph scales comparable.

The power extracted from the system is shown below in figure 2.16. Notice that there are points in the stationary cycle where the power generated is negative, which is not true in graph 2.11. The average power generated in this graph is still about 1.5 kW.

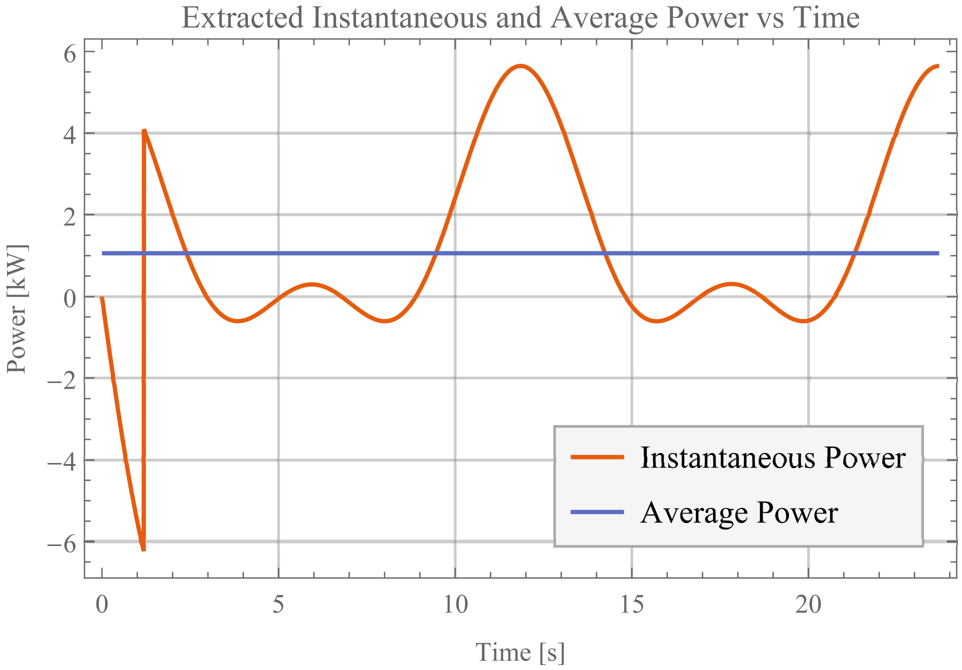

Figure 2.16: Instantaneous and average extracted power from the buoy vs time with initial conditions $(x0, v0) = (0, 0)$

The co-state graphs are provided below in figure 2.17 to prove that the simulation is still on a singular arc. This is true even though the initial condition $x0 = 0$ in this simulation is different from the optimal simulation of $x0 \approx 0.273$ used above. Also, the power extracted in figure 2.16 is less than figure 2.11. Still, once the system leaves bang-bang control and starts using the singular arc control law, the co-state constraints are line-on-line with the evolved co-states. This proves that the system is on a singular arc.

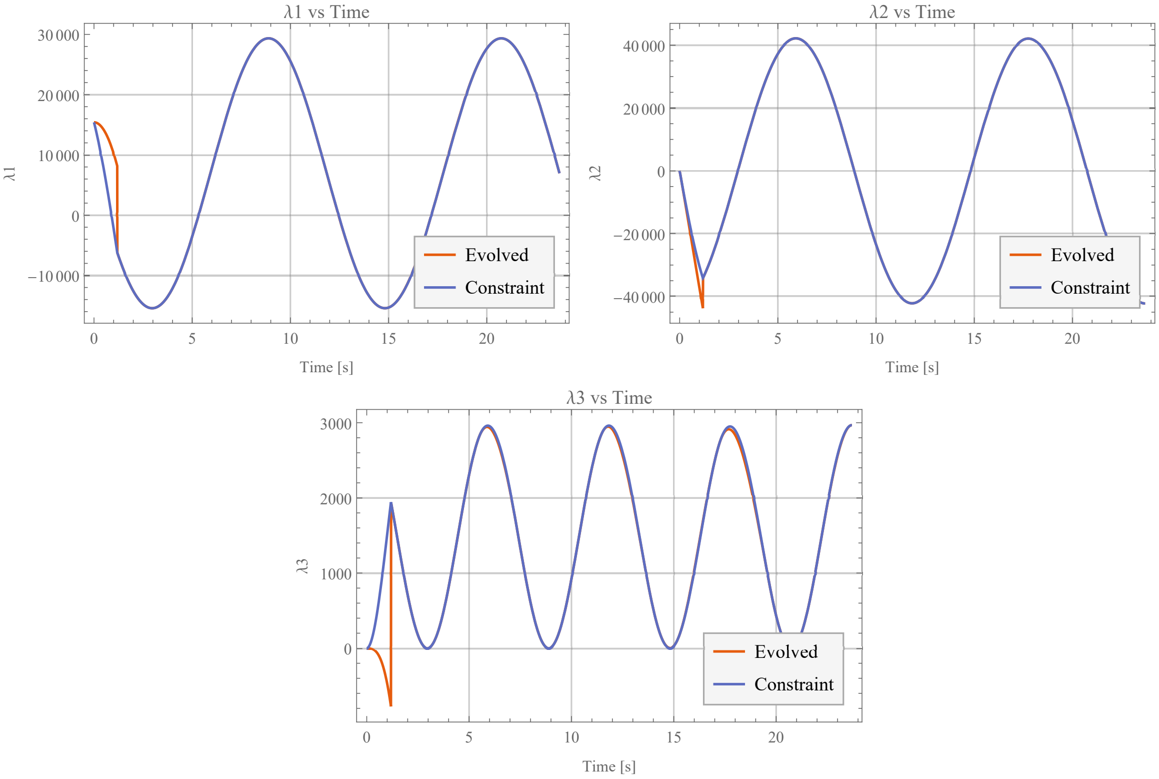

Figure 2.17: Co-state numerically integrated (evolved) from the differential equation and calculated from the singular constraint with initial conditions $(x0, v0) = (0, 0)$

2.6 Application to Hour Glass Buoy

The general control law from equation 2.27 will be applied to a non-linear hourglass buoy. Then numerical simulation will be used to verify the performance of this system.

2.6.1 Application of General Control Law to Hourglass Buoy

A schematic representation of the hourglass buoy is provided below in figure 2.18.

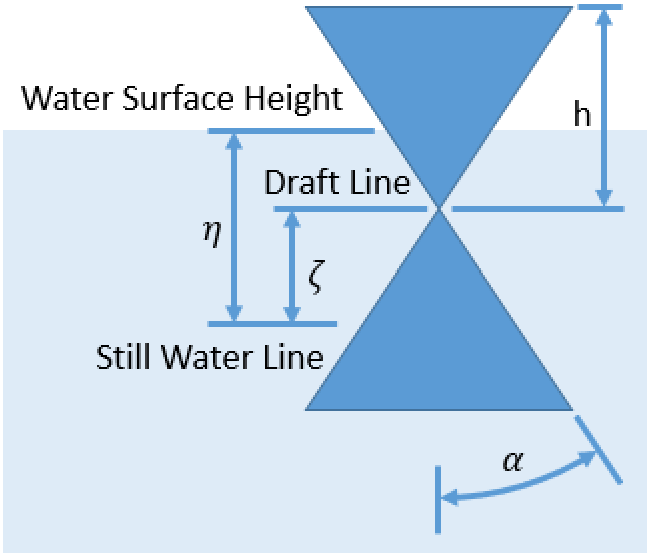
Water Surface Height
h
Draft Line
η
ζ
Still Water Line
α

Figure 2.18: Schematic representation of an hourglass buoy

The hydrostatic force on the buoy can be calculated by finding the submerged volume of the buoy V_{sub}. The hydrostatic force is given in equation 2.85. Note that a term for gravity has been included.

$$F_h = \rho \, g \, V_{sub} - m \, g \tag{2.85}$$

The submerged volume can be found as an integral of the cross-sectional area of the buoy. The cross-sectional area will be found as a function of buoy height, then this function can be integrated over the submerged height to find the submerged volume of the buoy.

The cross-sectional area of the buoy as a function of height is given below, where ζ is the position of the buoy with respect to the draft line.

$$S_w(z,\zeta) = \pi \tan(\alpha)^2[z-\zeta]^2 \tag{2.86}$$

The formula for the volume of a cone is provided below:

$$V_{cone} = \frac{1}{3}\pi \tan(\alpha)^2 h^3 \tag{2.87}$$

where h is the height of the cone.

The submerged volume can then be found as follows:

$$V_{sub} = V_{cone} + \int_{\zeta}^{\eta} S_w(z,\zeta)\, dz \tag{2.88}$$

The V_{cone} term accounts for the fact that at the draft line, half of the buoy is already submerged. The integral accounts for the change in the submerged volume due to the buoy position ζ and the height of the water from the draft line η.

Equations 2.85, 2.86, 2.87, and 2.88 can be combined to find the hydrostatic force on the buoy, which is shown below:

$$\begin{aligned} F_h(\zeta,\eta) &= \rho\, g\, V_{cone} + \rho\, g \int_{\zeta}^{\eta} \pi \tan(\alpha)^2 \,[z-\zeta]^2 \,dz - m\, g \\ &= \frac{1}{3}\rho\, g\, \pi \tan(\alpha)^2\, h^3 + \frac{1}{3}\rho\, g\, \pi \tan(\alpha)^2\, (\eta-\zeta)^3 - m\, g \end{aligned} \tag{2.89}$$

Through the density of water, the mass from the gravity term can be translated to a volume, which must be the volume of one of the cones. This can be reasoned by the fact that the draft line is defined so that one cone is fully submerged in still water. Thus the following is true:

$$m\, g = \rho\, g\, V_{cone} = \frac{1}{3}\rho\, g\, \pi \tan(\alpha)^2\, h^3 \tag{2.90}$$

Using this fact, the cone volume term and the gravity term cancel yielding the final equation for the hydrostatic force on the buoy:

$$\boxed{F_h(\zeta,\eta) = \frac{1}{3}\rho\, g\, \pi \tan(\alpha)^2\, (\eta-\zeta)^3} \tag{2.91}$$

Note that η is dependent on the time state T because η represents the water surface which is dependent on time. The wave height function should therefore actually be written as $\eta(T(t))$, however, the dependency has been dropped in the above equations for brevity.

If a stiffness-like variable is defined as $k = \frac{1}{3}\,\rho\, g\, \pi \tan(\alpha)^2$, then the similarities between the hourglass buoy model and the linear buoy model are evident.

$$F_l = k(\eta - \zeta) \tag{2.92}$$

$$F_h = k(\eta - \zeta)^3 \tag{2.93}$$

where F_l is the linear force model, and F_h is the hourglass force model.

According to the optimal control law, the derivative of the force with respect to the time state T is needed and is computed from equation 2.91 below. The full dependencies on the time state T and on time t has been written out for clarity.

$$\partial_{T(t)}\, F_h(\zeta(t),\, \eta(T(t))) = \pi\, \rho\, g\, \tan(\alpha)^2\, \left[\zeta(t) - \eta(T(t))\right]^2\, \dot{\eta}(T(t)) \tag{2.94}$$

Equations 2.91 and 2.94 can then be substituted directly into the optimal control law found in equation 2.27 to generate the following law relating to hourglass buoys. Finally the substitution $T(t) = t$ is made using equation 2.7. The time dependence of ζ is not included below, but it is implied. The time dependencies are used to denote that a function is non-autonomous.

$$\boxed{u_{sa}(t) = \frac{1}{3}\,\rho\, g\, \pi\, \tan(\alpha)^2\,(\eta(t) - \zeta)^3 - b\,\dot{\zeta} - \frac{m}{2b}\,\pi\,\rho\, g\, \tan(\alpha)^2\,(\zeta - \eta(t))^2\,\dot{\eta}(t)} \tag{2.95}$$

The control law that maximizes the energy extracted from an hourglass buoy was found directly from equation 2.27. Note that it is only valid if the system is on a singular arc.

Unfortunately, the procedure for generating a closed-form switching function for the linear system does not apply to the hourglass buoy. In the linear problem, equation 2.68 is only a function of the time state, so the integral of this function with respect to time has a closed-form solution. In the non-linear case, the force term on the right-hand side is dependent on both the time state as well as the position state variable. This means that there is no closed-form expression for this integral. The initial condition for this integral must be known at the start of the simulation to evolve the system, but the integral state is not known until the system is on the singular arc and the co-state constraint equations apply. More work needs to be done to find a general candidate switching function for non-linear models.

2.6.2 Searching for Singular Arcs

A method for searching for singular arcs was developed and demonstrated on the hourglass buoy model. In section 2.5.4, it was shown that the co-state constraints equations 2.22, 2.17, and 2.30 and the co-state evolution equations 2.13, 2.14, and 2.15 could be used to verify that a system was on a singular arc. If both the constraint and the evolution of the co-state differential equation produced the same result, then the system is on a singular arc. This is because the co-state constraints are derived from the stationary condition, so if the co-state constraints hold, then the stationary condition must hold.

While this test method can be used as a verification to ensure that the system is on a singular arc, it can be impractical as a search criterion. In practice, it is not clear how long to simulate the system for before a divergence is expected between the co-state evolution and the co-state constraint equations. Simulating the system for a long duration can also be computationally slow, as many simulations need to be run during the search.

An observation can be made that singular arcs should be periodic with the same period as the forcing wave. This observation leads to a practical search method. First, set up an error function that penalizes non-periodic trajectories. Next, choose an arbitrary state to check. Finally, simulate the system for one period, and check the error function. Standard numerical optimization techniques can be used to choose the next search point. Gradient-based methods were able to find two different singular arcs for the hourglass buoy case.

The error function to enforce periodicity was defined as:

$$\mathrm{err} = (x(0) - x(Tw))^2 + (v(0) - v(Tw))^2 \tag{2.96}$$

where Tw is the period of the wave.

2.6.3 Numerical Simulation of Hourglass Buoy

Using the numerical search method defined in section 2.6.2, two different singular arcs were found. The initial conditions for the arcs are $(x_0, v_0) = (-0.393072, 0.857953)$ and $(x_0, v_0) = (-0.0237669, 0.11256)$.

Table 2.2
Numerical values of quantities used in nonlinear simulations

Quantity	Value	Units	Description
g	9.81	$\mathrm{m/s^2}$	Acceleration due to gravity
ρ	1000	$\mathrm{kg/m^3}$	Density of water
m	109626	kg	Mass of the buoy
b	20000	N s/m	Linear viscous damping coefficient
k	π 9810	N/m	Spring force constant
a	0.5	m	Wave height
α	60	deg	Hourglass buoy angle
T_w	6	s	Period of wave field

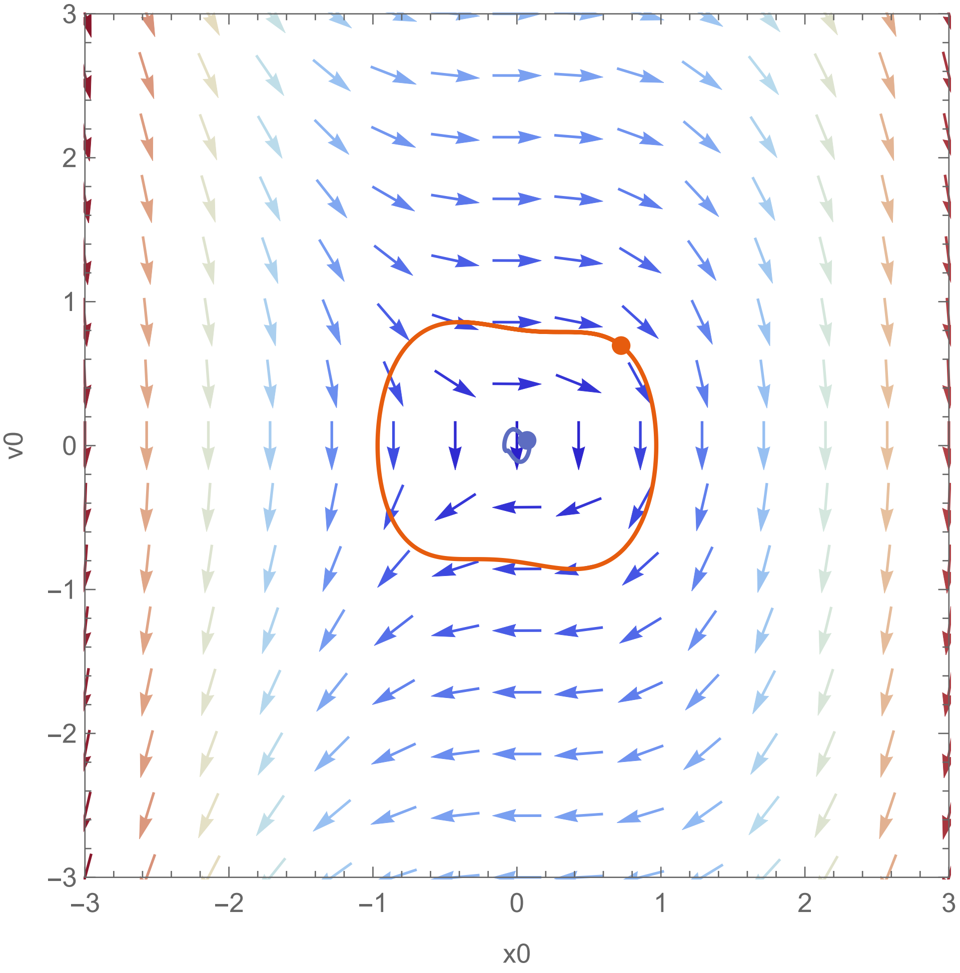

Figure 2.19: Phase space of hourglass buoy at t=7 s with two found singular arcs

Figure 2.19 shows the phase space of the nonlinear hourglass buoy system with two different singular arcs which were found using the numerical search method described in subsection 2.6.2. The current state of the system is represented by a dot. The trajectory of the system is represented by a curve.

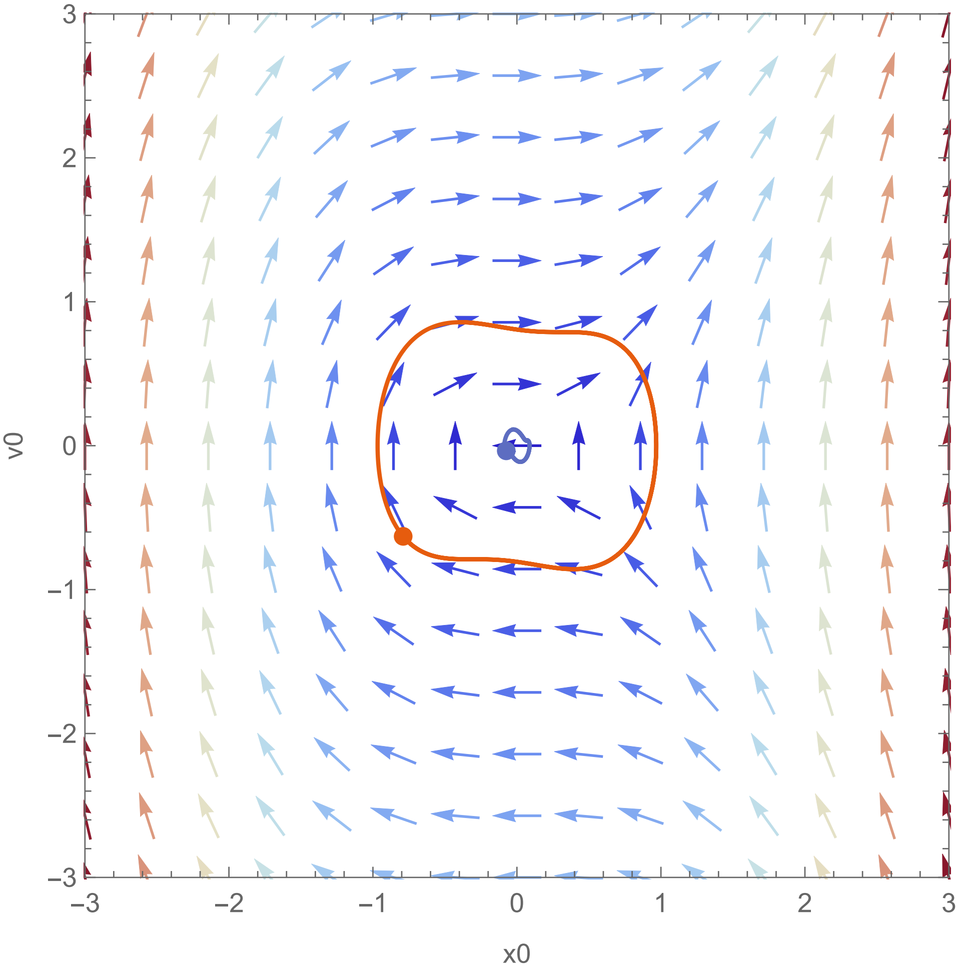

Figure 2.20: Phase space of hourglass buoy at t=10.5 s with two found singular arcs

The direction of the arrows in phase space is time-dependent. The phase space graph shows a stable side and an unstable side which flip sides with the period of the wave. Figure 2.20 shows when the orbits of the singular arcs are on the other side of the graph, and when the stable and unstable sides have flipped along the x0 axis.

The two singular arcs need to be analyzed to determine if they are optimal candidates.

The first arc to be analyzed will be the larger (orange) arc from figure 2.19. The velocity and the control force for the larger (orange) arc are shown in figure 2.21.

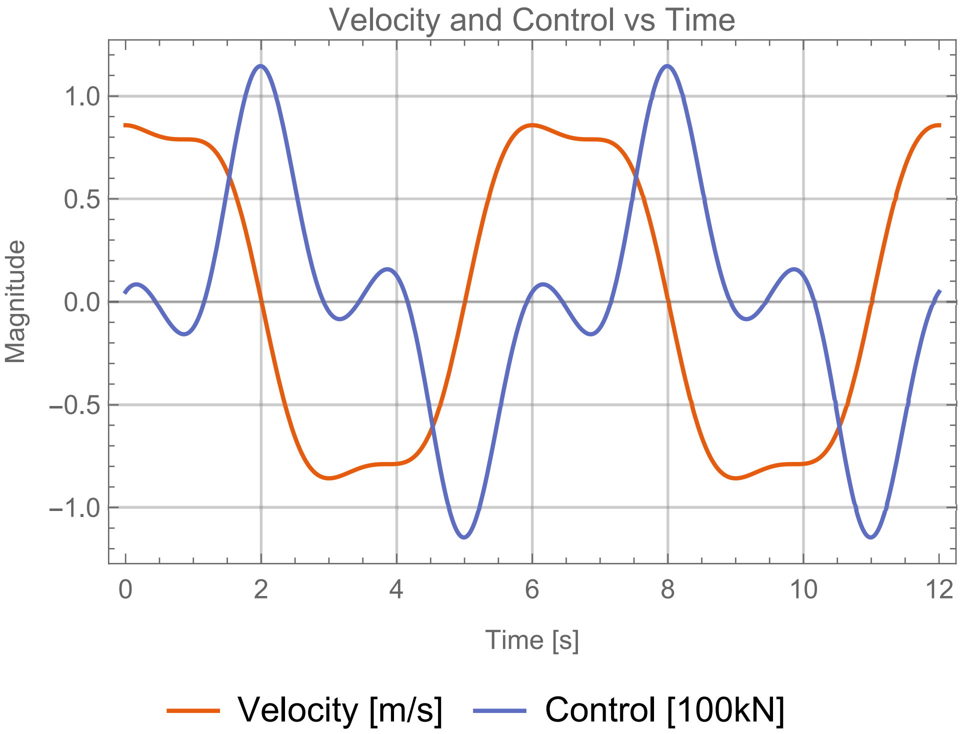

Figure 2.21: Velocity and control force for large (orange) singular arc orbit

The instantaneous and average power for the larger (orange) are shown in figure 2.22. This singular arc takes power to stay on, as can be seen by the fact that the average power is approximately -1.5 kW.

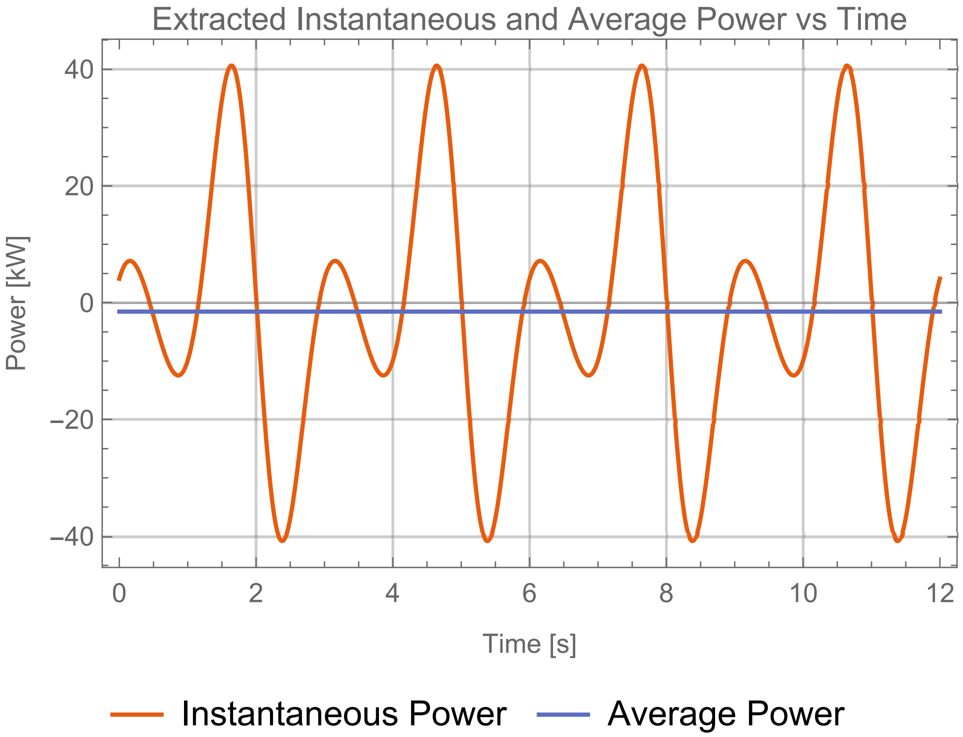

Figure 2.22: Instantaneous and Average power for large (orange) singular arc orbit

The trajectory is verified to be a singular arc by comparing the co-state equations and the co-state constraints in figure 2.23.

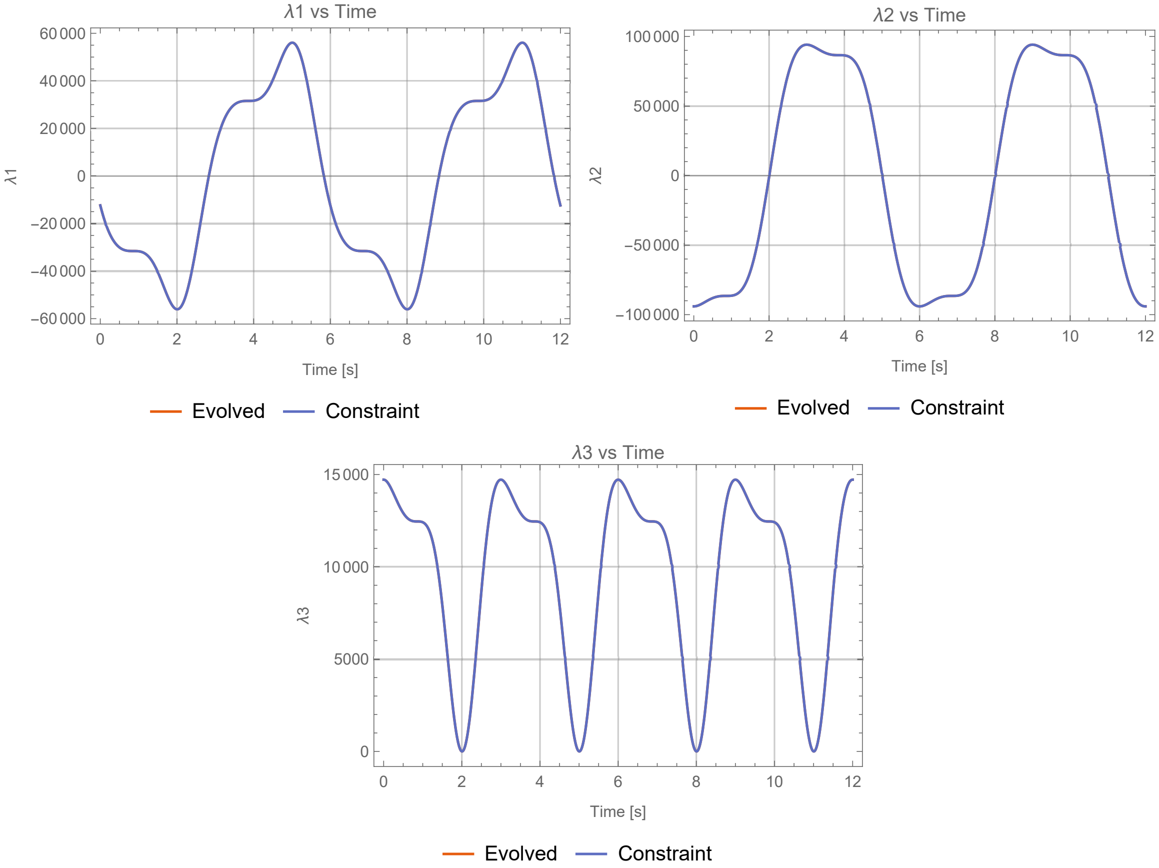

Figure 2.23: Co-state evolved vs constraint check for large (orange) singular arc orbit

The second arc to be analyzed will be the smaller (blue) arc from figure 2.19. The velocity and the control force for this arc are shown in figure 2.24.

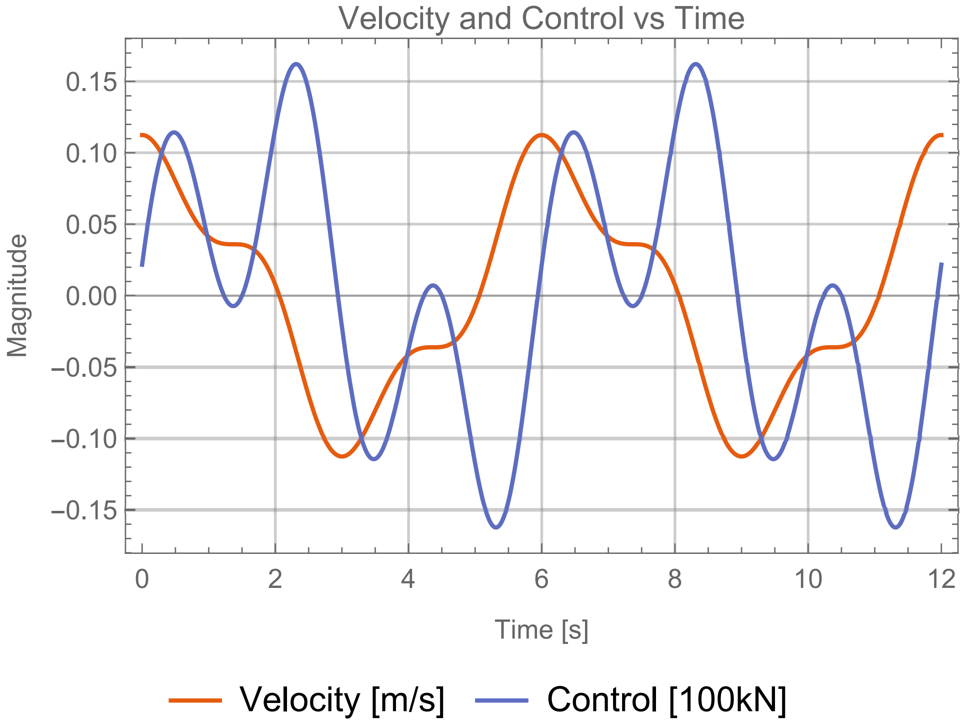

Figure 2.24: Velocity and control force for smaller (blue) singular arc orbit

The instantaneous and average power for the smaller (blue) are shown in figure 2.25. This singular arc takes does generate power, but the result is minuscule at approximately 70 watts. This makes sense as the velocities for this arc are small, and power generation is related to velocity.

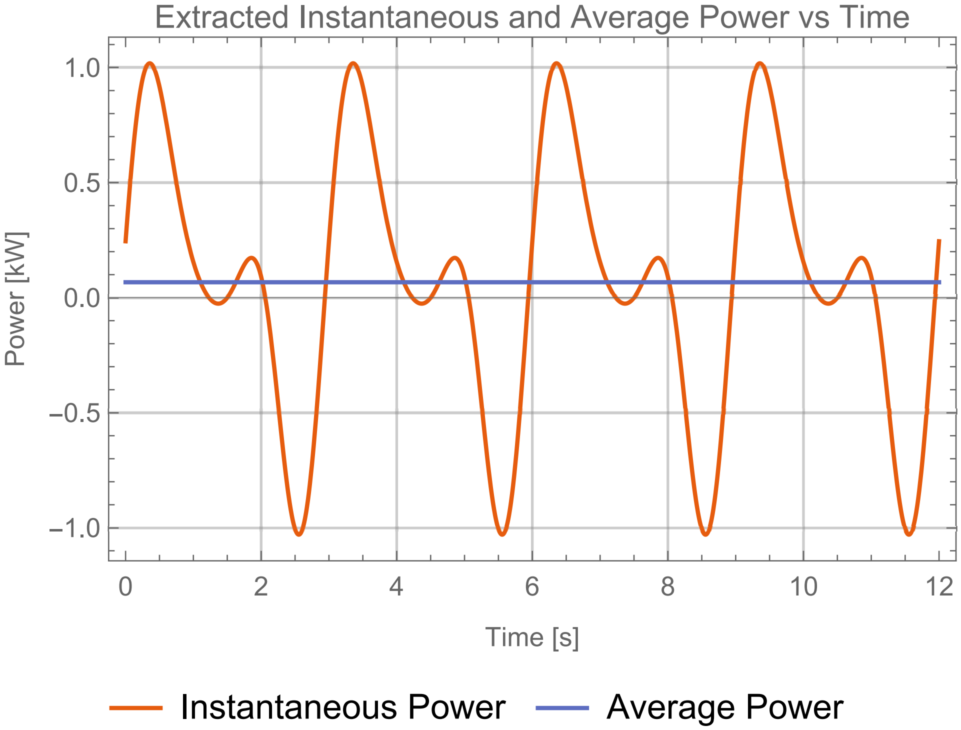

Figure 2.25: Velocity and control force for smaller (blue) singular arc orbit

The trajectory is verified to be a singular arc by comparing the co-state equations and the co-state constraints in figure 2.26.

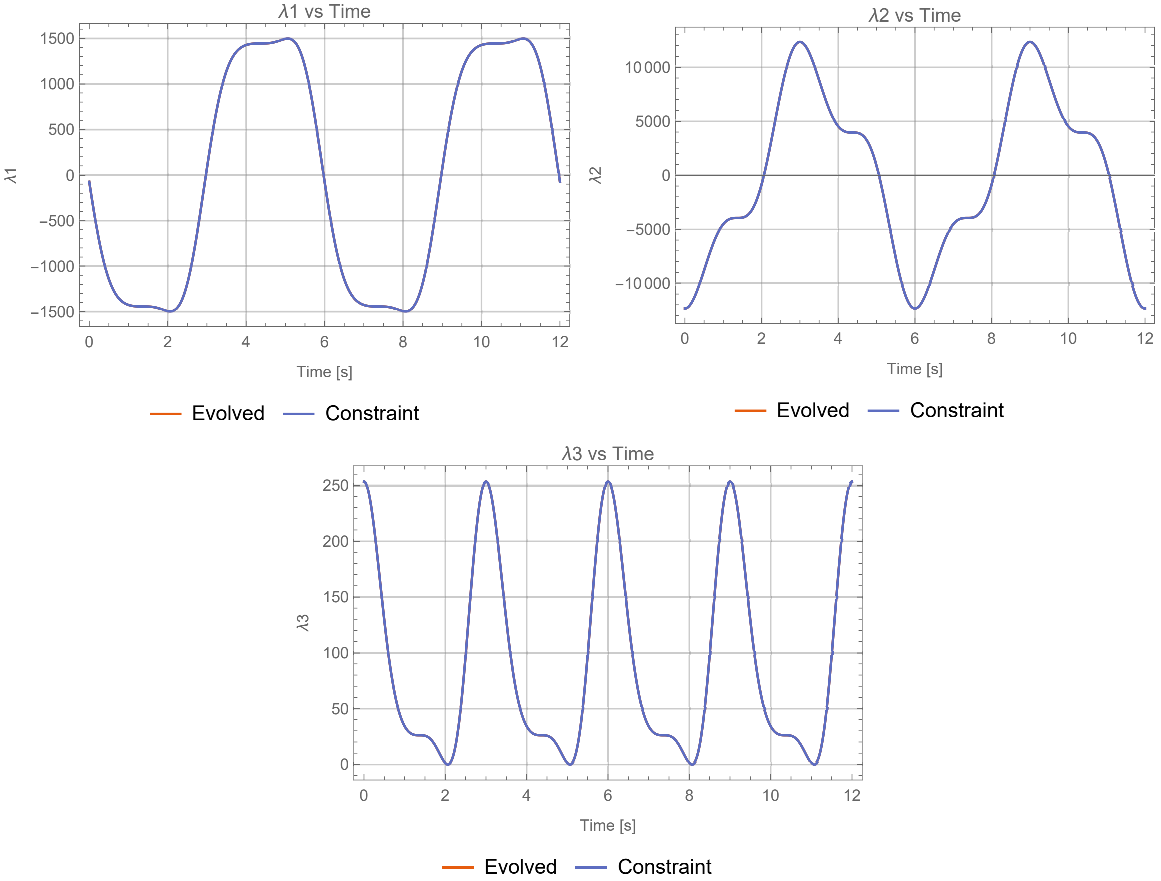

Figure 2.26: Velocity and control force for smaller (blue) singular arc orbit

Two singular arcs were found and analyzed, but it is unlikely that either are the optimal candidate. It is very possible that the search method used was unable to find optimal arc.

Chapter 3

Conclusions

Optimal control methods were explored for non-linear wave energy converters. A derivation of the optimal problem was provided, and the solution was explored for both linear and hourglass-shaped buoys.

3.1 Summary of Findings

Optimal control methods which maximize the power extracted from a certain class of non-linear wave energy converters were presented in this thesis. The class of non-linear wave energy converters considered were models where the non-linear force could be written in terms of the position state and the time state of the system. Allowing the time state to be included in the non-linear force term allows the term to be non-autonomous, which is necessary to model wave heights that evolve with time.

A general control law for the class of non-linear systems was found which maximizes the power generated from a system when it is on a singular arc. This general control law is directly applicable to any buoy model which falls within the class of non-linear models considered. The general control law is only valid when the system is on a singular arc.

This general control law was then applied to a linear buoy model. A switching function was defined which discerns whether the system is on a singular arc, and a bang-bang controller was defined to drive the system to the singular arc. Numerical analysis of the buoy model was performed which verifies the performance of the system. The behavior of the buoy both on and off the singular arc is demonstrated to be optimal through numerical simulation.

It is demonstrated that there are infinitely many singular arcs that the system can be on. Only one singular arc is optimal, which is demonstrated through simulation. A method to construct all possible singular arcs is shown, which is to set the position initial condition to any arbitrary value. This is justified through analysis of the switching function. The performance of two different singular arcs are compared - one which is optimal, and the other which starts at the arbitrarily chosen initial position of 0.

The general control law is applied to an hourglass-shaped buoy. A switching function is difficult to find for non-linear systems, so a numerical search is used to find initial conditions which are on the singular arc. Two singular arc candidates are found and analyzed. Neither generate significant power, so it is likely that neither are the optimal candidate.

3.2 Future Work

A systematic way of finding initial conditions which are on singular arcs for the general non-linear problem is needed. A method of finding switching functions that can be used for bang-bang control for non-linear systems is also needed.

If these are found to not be possible, more robust code for searching for the singular arcs and driving the system towards one of these arcs can be written.

Work also needs to be done to determine if there is some algorithm that can be used as a switching function to determine in which direction the system should travel to move toward the singular arc.

Finally, it would be interesting to develop a controller which used feedback to reject perturbations away from the optimal singular arc.

References

[1] Zou, S.; Abdelkhalik, O.; Robinett, R.; Bacelli, G.; Wilson, D. *Renewable energy* **2017**, *103*, 217–225.

[2] Conti, J. J.; Holtberg, P. D.; Beamon, J. A.; Schaal, A. M.; Ayoub, J.; Turnure, J. T. *US Energy Information Administration* **2014**, *2*.

[3] Korde, U. A.; Ringwood, J. *Hydrodynamic control of wave energy devices;* Cambridge University Press, 2016.

[4] Van Vuuren, D.; Nakicenovic, N.; Riahi, K.; Brew-Hammond, A.; Kammen, D.; Modi, V.; Nilsson, M.; Smith, K. *Current Opinion in Environmental Sustainability* **2012**, *4*(1), 18–34.

[5] Thorpe, T. *Wave power: moving towards commercial viability* **1999**, *26*, 50–120.

[6] McCormick, M. E. *Ocean wave energy conversion*, Dover Civil and Mechanical Engineering; Dover Publications: Mineola, NY, 2007.

[7] Falnes, J.; Budal, K. *Norw. Marit. Res., 6(4), 2-11, (1978)* **1978**.

[8] Giorgi, G.; Ringwood, J. V. *Journal of Ocean Engineering and Marine Energy* **2017**, *3*(1), 21–33.

[9] Hals, J.; Falnes, J.; Moan, T. *Journal of Offshore Mechanics and Arctic Engineering* **2011**, *133*(3).

[10] Falnes, J.; Kurniawan, A. *Ocean waves and oscillating systems: linear interactions including wave-energy extraction*, Vol. 8; Cambridge university press, 2020.

[11] Kasturi, P.; Dupont, P. *Journal of Sound and vibration* **1998**, *215*(3), 499–509.

[12] Lewis, F. L.; Vrabie, D.; Syrmos, V. L. *Optimal control;* John Wiley & Sons, 2012.

[13] Sage, A. P.; White, C. C. *Optimum systems control;* Prentice Hall, 1977.

[14] Scardina, J. A. *An investigation of singular optimal control problems* PhD thesis, Georgia Institute of Technology, **1968**.

[15] Aronna, M. S. *Second order analysis of optimal control problems with singular arcs. Optimality conditions and shooting algorithm.* PhD thesis, Ecole Polytechnique X, **2011**.

[16] Kelley, H. J. *AIAA Journal* **1964**, *2*(8), 1380–1382.

[17] Bryson, A. E.; Ho, Y.-C. *Applied optimal control: optimization, estimation, and control;* Routledge, 2018.

[18] Garcia-Rosa, P. B.; Bacelli, G.; Ringwood, J. V. *Energies* **2015**, *8*(12), 13672–13687.

[19] Garcia-Rosa, P. B.; Ringwood, J. V. *IEEE Transactions on Sustainable Energy* **2015**, *7*(1), 419–426.

[20] Garcia-Teruel, A.; Forehand, D. *Renewable and Sustainable Energy Reviews* **2021**, *139*, 110593.

[21] Wilson, D. G.; Robinett III, R. D.; Bacelli, G.; Abdelkhalik, O.; Coe, R. G. *Journal of Marine Science and Engineering* **2020**, *8*(2), 84.

[22] Houssein Yassin, Gordon Parker, D. W. *Energies* **2022**.

[23] Zou, S.; Abdelkhalik, O. *IEEE Journal of Oceanic Engineering* **2020**, *46*(3), 879–890.

Appendix A

Differentiable Approximations to Piecewise Linear Functions

Often it is desirable to include piecewise linear functions in a dynamic system model. However, the method above requires that all functions in the non-linear force model are differentiable. Differentiable approximations to any piecewise linear function can be built to an arbitrarily close approximation using the method described below.

The core insight to this approximation method is that the derivative of any piecewise linear function will be some stair step function.

The derivative of any piecewise linear function can therefore be represented as some sum and product of shifted and scaled step(x) functions. These step(x) functions can

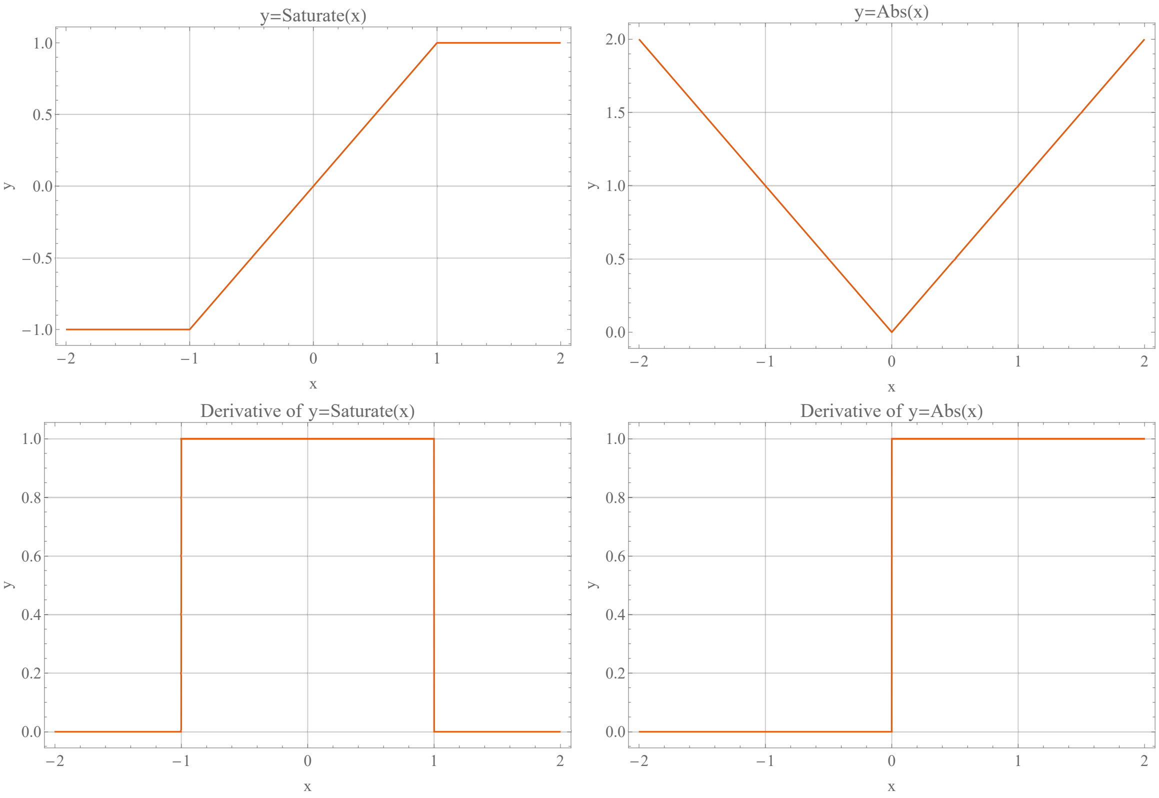

Figure A.1: Saturate(x) and Abs(x) and their derivatives

then be approximated as sigmoid(x) functions. Finally the approximated derivative function can be integrated to build the approximation of the desired function.

The equation for a sigmoid function is given below:

$$\text{sigmoid}(x) = \frac{e^{kx}}{1 + e^{kx}} \tag{A.1}$$

In the sigmoid function, k is a smoothing parameter such that:

$$\lim_{k \to \infty} \frac{e^{kx}}{1 + e^{kx}} = \text{step}(x) \tag{A.2}$$

The figure below shows how a sigmoid(x) functions can approximate a step(x) arbitrarily closely.

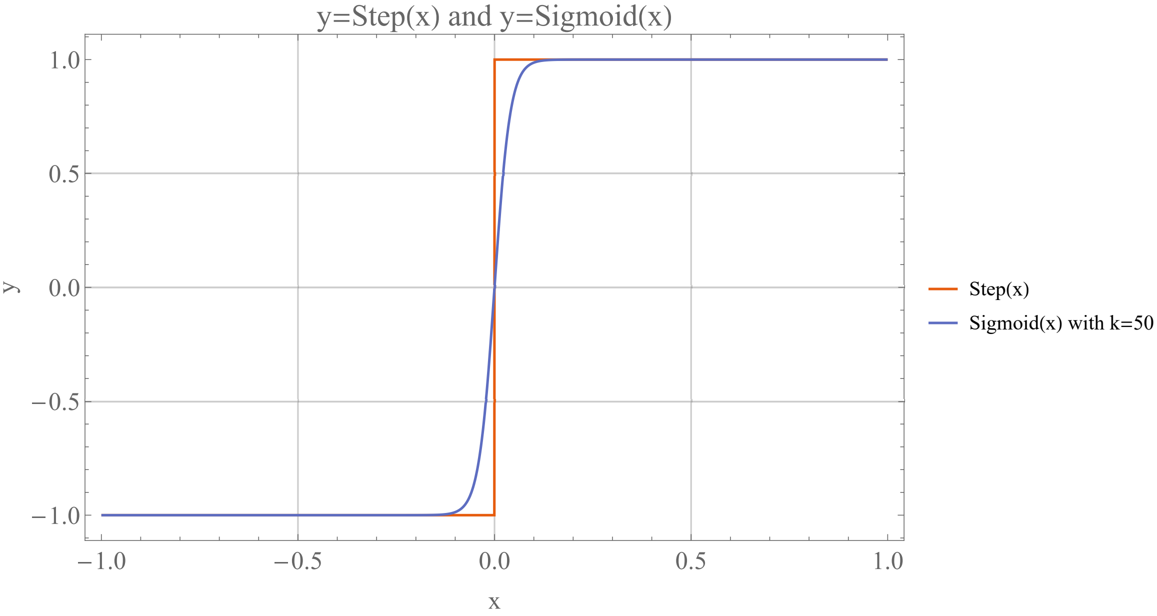

Figure A.2: Step(x) function overlaid against Sigmoid(x) curve with k=50

While the approximation functions generated using this method can be cumbersome to work with by hand, they pose no issue to a computer algebra system or a numerical solver software package.

A.1 Approximation of the Saturate Function

The derivative of the saturate function (shown in figure A.1) can be represented as step functions in the following way:

$$\partial_x \operatorname{saturate}(x) = \operatorname{step}(1-x) * \operatorname{step}(1+x) \tag{A.3}$$

This can be approximated by replacing the step functions with sigmoids:

$$\begin{aligned}\partial_x \operatorname{saturate}(x) &\approx \operatorname{sigmoid}(1-x) * \operatorname{sigmoid}(1+x) \\ &\approx \frac{e^{k(1-x)}}{1+e^{k(1-x)}} * \frac{e^{k(1+x)}}{1+e^{k(1+x)}}\end{aligned} \tag{A.4}$$

Finally equation A.4 can be integrated to produce an approximation of the saturate(x) function as follows:

$$\begin{aligned}\operatorname{saturate}(x) &\approx \int \frac{e^{k(1-x)}}{1+e^{k(1-x)}} * \frac{e^{k(1+x)}}{1+e^{k(1+x)}}\,dx \\ &\approx \frac{e^{2k}}{k(e^{2k}-1)}\left[\ln(e^{k}+e^{-kx}) - \ln(1+e^{k(1-x)})\right]\end{aligned} \tag{A.5}$$

Therefore a good approximation to the saturate function is the following equation:

$$\boxed{\text{saturate}(x) \approx \frac{e^{2k}}{k(e^{2k}-1)} \left[\ln(e^{k}+e^{-kx}) - \ln(1+e^{k(1-x)})\right]} \tag{A.6}$$

A.2 Approximation of the Abs Function

The derivative of the abs function (shown in figure A.1) can be written as follows:

$$\partial_x \operatorname{abs}(x) = 2 \ \text{step}(x) - 1 \tag{A.7}$$

This can be approximated as:

$$\begin{aligned} \partial_x \operatorname{abs}(x) &\approx 2 \ \text{sigmoid}(x) - 1 \\ &\approx \frac{2 \ e^{kx}}{1+e^{kx}} - 1 \end{aligned} \tag{A.8}$$

The approximation can be integrated as follows:

$$\begin{aligned} \text{abs}(x) &\approx \int \frac{2\ e^{kx}}{1+e^{kx}} - 1\,dx \\ &= \frac{2}{k}\ln[1+e^{kx}] - x \end{aligned} \tag{A.9}$$

Therefore a good approximation to the abs function is the following equation:

$$\boxed{\text{abs}(x) \approx \frac{2}{k}\ln[1+e^{kx}] - x} \tag{A.10}$$

Appendix B

Mathematica Code

```
export[filename_, object_] :=
 Export[FileNameJoin[{NotebookDirectory[], "Figures", filename <> #}], object] & /@ {".eps", ".png"}
```

The default color palette comes from the “scientific theme” used in Mathematica
A plot command is defined to make consistent themed plots from this code.

```
defaultColors = ColorData[108, "ColorList"];
color[idx_] := Module[{mod},
  mod = Mod[idx - 1, First[Dimensions[defaultColors]]] + 1;
  Part[defaultColors, mod]
 ]

prep[qty_] := qty //. Join[subs, soln]
plot[qty_, opts___] := Plot[
  Evaluate[prep[qty]], {t, 0, tMax},
  opts,
  PlotStyle → defaultColors,
  GridLines → Automatic, PlotRange → All,
  Frame → True, ImageSize → Medium
 ]
```

genSoln generates a series of trajectories based on a vector of initial conditions. It is configured using a series of global variables which are listed below.

`tMac`	The max time to simulate to
`ctl`	The control law to use. Generally u[t] → uSa or u[t] → 0
`force`	The force model to use. Generally forceLinear or forceHourglass
`inits`	A list of initial conditions for the states.
`soln`	The results from the calculation

The co-state initial conditions are assumed to start on a singular arc. The initial conditions are generated using the co-state constraint equations.

genSolnSwitched is similar to genSoln, however includes extra logic to implement bang-bang control.
A switching rule is defined which changes a mode variable depending on whether the control should be the min, max, or singular control. The method is changed to stiffnessSwitching which is necessary for the integrator to make it through the problem.
Note that this method seems to introduce some numerical error. While the percentage error is low compared to the regular method, certain functions like the Hamiltonian (which end up being sensitive to this kind of error) will evaluate to non-constant expressions.

```
Clear[genSoln]
genSoln := DynamicModule[{initIdx},
  Dynamic[initIdx];
  initIdx = 0;
  solns = Monitor[MapIndexed[Module[{ret},
      ret = Function[{init, idx}, Last[NDSolve[Join[
            Thread[dX == D[H, {Λ}]],
            Thread[-dΛ == D[H, {X}]],
            Thread[(X /. t → 0) == init],
            costateConstraints //. Join[{t → 0, Rule → Equal}]
           ] //. subs,
          Join[X, Λ], {t, 0, tMax}
         ]]]; initIdx += 1; ret
     ], inits],
    ToString[NumberForm[N[          initIdx
                          ──────────────────────── * 100], {∞, 2}]] <> "% complete"
                          First[Dimensions[inits]]
   ]]

Clear[genSolnSwitched]
genSolnSwitched := DynamicModule[{currentTime, initIdx},
  Dynamic[currentTime]; currentTime = 0;
  Dynamic[initIdx]; initIdx = 0;
  solns = Monitor[MapIndexed[Module[{ret},
      ret = Function[{init, idx}, Last[NDSolve[Join[
            Thread[dX == D[H, {Λ}]],
            Thread[-dΛ == D[H, {X}]],
            Thread[(X /. t → 0) == init],
            costateConstraints //. Join[{t → 0, Rule → Equal}],
            switchRule
           ] //. subs,
          Join[X, Λ, {mode[t]}], {t, 0, tMax},
          DiscreteVariables → mode,
          Method → "StiffnessSwitching",
          EvaluationMonitor :→ (currentTime = t;)
         ]]]; initIdx += 1; ret
     ], inits],
    ToString[currentTime] <> " " <>
     ToString[NumberForm[N[          initIdx
                           ──────────────────────── * 100], {∞, 2}]] <> "% complete"
                           First[Dimensions[inits]]
   ]]
```

makePlots generates a series of plots that we are usually interested in for these kinds of systems.

```
Clear[makePlots]
makePlots := Module[{p1, p2, avgPwr, p3, p4, p5, p6},


  p1 = plot[{x[t], v[t]},
    FrameLabel → {"Time [s]", "Magnitude"},
    PlotLabel → "Position and Velocity vs Time",
    PlotLegends → Placed[{"Position [m]", "Velocity [m/s]"}, Below]
   ];

  p2 = plot[{v[t], u[t] / 10000},
    FrameLabel → {"Time [s]", "Magnitude"},
    PlotLabel → "Velocity and Control vs Time",
    PlotLegends → Placed[{"Velocity [m/s]", "Control [10kN]"}, Below]
   ];
  avgPwr = 1/tMax Quiet[NIntegrate[prep[v[t] * u[t] / 1000], {t, 0, tMax}]];
  p3 = plot[{v[t] * u[t] / 1000, avgPwr},
    FrameLabel → {"Time [s]", "Power [kW]"},
    PlotLabel → "Extracted Instantaneous and Average Power vs Time",
    PlotLegends → Placed[{"Instantaneous Power", "Average Power"}, Below]
   ];

  p4 = plot[H,
    FrameLabel → {"Time [s]", "H"},
    PlotLabel → "Hamiltonian vs Time"
   ];

  p5 = plot[ξ[t],
    PlotLabel → "Switching Function vs Time",
    FrameLabel → {"Time [s]", "ξ"}
   ];

  p6 = Grid[{{
      plot[{λ1[t], λ1[t] /. costateConstraints}, PlotLabel → "λ1 vs Time",
        FrameLabel → {"Time [s]", "λ1"}, PlotLegends → Placed[{"Evolved", "Constraint"}, Below]],
      plot[{λ2[t], λ2[t] /. costateConstraints}, PlotLabel → "λ2 vs Time",
        FrameLabel → {"Time [s]", "λ2"}, PlotLegends → Placed[{"Evolved", "Constraint"}, Below]]
     }, {
      plot[{λ3[t], λ3[t] /. costateConstraints}, PlotLabel → "λ3 vs Time",
        FrameLabel → {"Time [s]", "λ3"}, PlotLegends → Placed[{"Evolved", "Constraint"}, Below]],
      SpanFromLeft
     }}];

  {p1, p2, p3, p4, p5, p6}
 ]
```

```
Clear[render]
render[T0_] := Module[{rangeSubs, xMin, xMax, vMin, vMax, vp, pp, gp},
  rangeSubs = Thread[{xMin, xMax, vMin, vMax} -> Flatten[range]];
  (*  vector plot *)
  vp = VectorPlot[
    Evaluate[F[[1 ;; 2]] //. Join[subs, {v[t] → v, x[t] → x, T[t] → T0}]],
    Evaluate[{x, xMin, xMax} /. rangeSubs], Evaluate[{v, vMin, vMax} /. rangeSubs],
    VectorScale → {0.04, Automatic, None},
    VectorColorFunction → Function[{x, y, vx, vy, n}, ColorData["ThermometerColors"][n]],
    PlotRange → range,
    FrameLabel → {"x0", "v0"}
   ];
  (*  parametric plot of trajectores *)
  pp = ParametricPlot[Evaluate[{x[t], v[t]} //. solns], {t, 0, T0}, PlotStyle → defaultColors];
  (*  points at head of trajectories *)
  gp = Graphics[Flatten[MapIndexed[Function[{soln, idx}, {PointSize[Large],
        color[idx[[1]]], Point[{x[t], v[t]}] //. Join[soln, {t → T0}]}], solns]]];
  Show[vp, pp, gp]
 ]
animate := Animate[render[T0], Evaluate[{T0, 10^-6, tMax} //. nVals], DefaultDuration → tMax]
```

Setup Optimal Control Problem

Setup the optimal control problem and solve for the singular arc control. Also setup the force and wave models. Finally, solve for the co-state constraints.

```
X = {x[t], v[t], T[t]};
Λ = {λ1[t], λ2[t], λ3[t]};
dX = D[X, t];
dΛ = D[Λ, t];

(* differential equations *)
{
   x'[t] == v[t],
   m v'[t] + b v[t] == Fe[x[t], T[t]] - u[t],
   T'[t] == 1
  };

F = dX /. Solve[%, dX][[-1]] // Simplify;

(* lagrangian and hamiltonian *)
Φ = -u[t] v[t];
H = Φ + Λ.F;

(* necessary conditions for optimality *)
D[H, u[t]] == 0;
sys = Join[
    Thread[dX == D[H, {Λ}]],
    Thread[-dΛ == D[H, {X}]],
    {%, D[%, t]}
   ];

(* solve for costate constraints *)
Join[{0 == H}, sys[[{2, 5, 7, 8}]]];
Eliminate[%, {v'[t], λ2′[t]}];
costateConstraints = Solve[%, {λ1[t], λ2[t], λ3[t]}] // Last;

costateConstraints[[{1}]] //. {Rule → Equal};
D[%, t];
Join[%, sys[[{1, 2, 3, 4}]]];
Eliminate[%, {x'[t], v'[t], T'[t], λ1′[t]}] //. costateConstraints[[{2}]];

(* solve for singular arc control *)
uSa[t_] = u[t] /. Solve[%, u[t]] // Last // FullSimplify;
```

```
(* numerical values taken from Houssein's paper *)
nVals = {
    g → 981 / 100, ρ → 1000, ϵ → 10^-6, a → 5 / 10,
    m → 50 376 + ma, ma → 59 250, b → 20 000, α → 60 * π / 180,
    k -> 1/3 π ρ g Tan[α]^2, uMax → 20 000, Tw -> 2 π / Sqrt[k / m]
   };

(* wave model *)
η[T] → a Cos[2 π / Tw T];
wave = {%, D[%, T]} //. {f_[T] → f[T_], Rule → RuleDelayed};

(* force models *)
Fe[x, T] → -k (x - η[T]);
forceLinear = {%, D[%, x], D[%, T]} //. {f_[x, T] → f[x_, T_], Rule → RuleDelayed};

Fe[x, T] → -k (x - η[T])^3;
forceHourglass = {%, D[%, x], D[%, T]} //. {f_[x, T] → f[x_, T_], Rule → RuleDelayed};
```

Linear System, Initial Conditions on Singular Arc

This is a simulation of the linear system which starts on the singular arc were x0=0.

```
tMax = Tw //. nVals;
ctl = {u[t_] :> uSa[t]};
force = forceLinear;
switching = {ξ[t_] :> v[t] - k/(2 b) η[T[t]]};
inits = {{0, a k/(2 b), 0}};
subs = Join[ctl, force, wave, nVals, switching];


genSoln;
soln = solns[[1]];
makePlots // TableForm
```

Linear System, Initial Conditions off Singular Arc (bang bang)

Uses bang-bang control to go to the singular arc
Two different singular arcs are simulated. The first is very similar to the one above. The second is just an arbitrary arc where the initial conditions are (0,0) and where the bang-bang control drives to the nearest arc.

```
tMax = 2 Tw //. nVals;
ctl = {u[t_] ⧴ uMax * mode[t] + uSa[t] * (1 - Abs[mode[t]])};
force = forceLinear;
inits = {
   {0.27335446434033694`, 0, 0}, (* close to same singular arc as ideal case above *)
   {0, 0, 0}                     (* off center singular arc *)
  };
                          k
switching = {ξ[t_] ⧴ v[t] - ─── η[T[t]]};
                          2 b
switchRule = {
   WhenEvent[ξ[t] > ϵ, {mode[t] → 1}],
   WhenEvent[ξ[t] < -ϵ, {mode[t] → -1}],
   WhenEvent[ξ[t] == 0, Evaluate[Join[{mode[t] → 0}, costateConstraints //. subs]]],
   {mode[0] == Piecewise[{{1, ξ[0] > ϵ}, {-1, ξ[0] < -ϵ}}, 0]}
  };
subs = Join[ctl, force, wave, switching, nVals];

genSolnSwitched;
soln = solns[[1]]; (* close to same singular arc as ideal case above *)
makePlots // TableForm

soln = solns[[2]]; (* off center singular arc *)makePlots // TableForm
```

Nonlinear (Hourglass) System

Set wave period to be shorter so that there is a stable solution

```
nVals = nVals /. {(Tw → _) :→ (Tw → 6)};
ctl = {u[t_] :→ uSa[t]};
force = forceHourglass;
subs = Join[ctl, force, wave, nVals];
```

Search for the arcs by looking for stable orbits that are one period long
A stable orbit must have the same state at the beginning and the end of one period

```
Clear[stableSearch]
stableSearch[x0_?NumericQ, v0_?NumericQ] := Module[{tMax, dSys, soln, err},
  tMax = Tw //. nVals;
  dSys = Join[
     Thread[dX == F],
     {x[0] == x0, v[0] == v0, T[0] == 0}
    ] //. subs;
  soln = NDSolve[dSys, X, {t, 0, tMax}, Method → "StiffnessSwitching"][[-1]] /.
    {x[t] → x[t_], v[t] → v[t_], T[t] → T[t_], Rule → RuleDelayed};
  err = ((x[0] - x[Tw])^2 + (v[0] - v[Tw])^2) //. Join[nVals, soln];
  err
 ]

initialGuesses = {{-1, -1}, {-1, 0}, {-1, 1}, {0, -1}, {0, 0}, {0, 1}, {1, -1}, {1, 0}, {1, 1}};
idx = 0;
Dynamic[idx];
stableInits = Monitor[MapIndexed[
     Function[{s, i}, Block[{ret}, ret = FindMinimum[stableSearch[x0, v0],
          {{x0, First[s]}, {v0, Last[s]}}, Method → "PrincipalAxis"] // Quiet;
       idx = i[[1]]; ret]],
     initialGuesses
    ], idx];
stableInits = SortBy[stableInits, #[[1]] &];
stableInits // TableForm
```

Select initial conditions from the list of stable orbits above

```
inits = Function[idx, {x0, v0, 0} /. stableInits[[idx, 2]]][{1, 4}]
```

```
{{-0.393072, 0.857953, 0}, {-0.0237669, 0.11256, 0}}
```

Simulate and animate system

```
tMax = 2 Tw //. nVals;
range = {{-3, 3}, {-3, 3}};

genSoln;
animate

render[7]
export["nonlinear_phasespace_start", %]
render[10.5]
export["nonlinear_phasespace_end", %]
```

```
soln = solns[[1]];

plot[{v[t], u[t] / 100000},
 FrameLabel → {"Time [s]", "Magnitude"},
 PlotLabel → "Velocity and Control vs Time",
 PlotLegends → Placed[{"Velocity [m/s]", "Control [100kN]"}, Below]
]
export["nonlinear_s1_velandctl", %]

          1
avgPwr = ──── Quiet[NIntegrate[prep[v[t] * u[t] / 1000], {t, 0, tMax}]];
         tMax
plot[{v[t] * u[t] / 1000, avgPwr},
 FrameLabel → {"Time [s]", "Power [kW]"},
 PlotLabel → "Extracted Instantaneous and Average Power vs Time",
 PlotLegends → Placed[{"Instantaneous Power", "Average Power"}, Below]
]
export["nonlinear_s1_pwr", %]

Grid[{{
   plot[{λ1[t], λ1[t] /. costateConstraints}, PlotLabel → "λ1 vs Time",
    FrameLabel → {"Time [s]", "λ1"}, PlotLegends → Placed[{"Evolved", "Constraint"}, Below]],
   plot[{λ2[t], λ2[t] /. costateConstraints}, PlotLabel → "λ2 vs Time",
    FrameLabel → {"Time [s]", "λ2"}, PlotLegends → Placed[{"Evolved", "Constraint"}, Below]]
  }, {
   plot[{λ3[t], λ3[t] /. costateConstraints}, PlotLabel → "λ3 vs Time",
    FrameLabel → {"Time [s]", "λ3"}, PlotLegends → Placed[{"Evolved", "Constraint"}, Below]],
   SpanFromLeft
  }}]
export["nonlinear_s1_costate", %]

soln = solns[[2]];

plot[{v[t], u[t] / 100000},
 FrameLabel → {"Time [s]", "Magnitude"},
 PlotLabel → "Velocity and Control vs Time",
 PlotLegends → Placed[{"Velocity [m/s]", "Control [100kN]"}, Below]
]
export["nonlinear_s2_velandctl", %]

          1
avgPwr = ──── Quiet[NIntegrate[prep[v[t] * u[t] / 1000], {t, 0, tMax}]];
         tMax
plot[{v[t] * u[t] / 1000, avgPwr},
 FrameLabel → {"Time [s]", "Power [kW]"},
 PlotLabel → "Extracted Instantaneous and Average Power vs Time",
 PlotLegends → Placed[{"Instantaneous Power", "Average Power"}, Below]
]
export["nonlinear_s2_pwr", %]

Grid[{{
   plot[{λ1[t], λ1[t] /. costateConstraints}, PlotLabel → "λ1 vs Time",
    FrameLabel → {"Time [s]", "λ1"}, PlotLegends → Placed[{"Evolved", "Constraint"}, Below]],
   plot[{λ2[t], λ2[t] /. costateConstraints}, PlotLabel → "λ2 vs Time",
    FrameLabel → {"Time [s]", "λ2"}, PlotLegends → Placed[{"Evolved", "Constraint"}, Below]]
  }, {
   plot[{λ3[t], λ3[t] /. costateConstraints}, PlotLabel → "λ3 vs Time",
    FrameLabel → {"Time [s]", "λ3"}, PlotLegends → Placed[{"Evolved", "Constraint"}, Below]],
   SpanFromLeft
  }}]
export["nonlinear_s2_costate", %]
```